

Changes in the expression of the type 2 diabetes-associated gene *VPSI3C* in the
 β cell are associated with glucose intolerance in humans and mice

Zenobia B. Mehta¹, Nicholas Fine¹, Timothy J. Pullen¹, Matthew C. Cane¹, Ming Hu¹,
Pauline Chabosseau¹, Gargi Meur¹, Antonio Velayos-Baeza², Anthony P. Monaco²,
Lorella Marselli³, Piero Marchetti³ and Guy A. Rutter^{1*}

¹Section of Cell Biology and Functional Genomics, Imperial College London, Du Cane Road
W12 0NN, London, UK

²Wellcome Trust Centre for Human Genetics Roosevelt Drive, OX3 7BN, Oxford, UK

³Department of Clinical and Experimental Medicine, University of Pisa, Pisa, Italy.

Running head

Glucose homeostasis in β cell-selective *VpsI3c* null mice

*Correspondence to Professor Guy A. Rutter, g.rutter@imperial.ac.uk

21 **Abstract**

22 Single nucleotide polymorphisms (SNPs) close to the *VPS13C*, *C2CD4A* and *C2CD4B* genes on
23 chromosome 15q are associated with impaired fasting glucose and increased risk of type 2 diabetes.
24 eQTL analysis revealed an association between possession of risk (C) alleles at a previously-
25 implicated causal SNP, rs7163757, and lowered *VPS13C* and *C2CD4A* levels in islets from female
26 ($n=40$; $p<0.041$) but not male subjects. Explored using promoter-reporter assays in β and other cell
27 lines, the risk variant at rs7163757, lowered enhancer activity. Mice deleted for *Vps13c* selectively in
28 the β cell were generated by crossing animals bearing a *floxed* allele at exon 1 to mice expressing *Cre*
29 recombinase under *Ins1* promoter control (Ins1Cre). Whilst *Vps13c*^{fl/fl}::Ins1Cre (β *Vps13c*KO) mice
30 displayed normal weight gain compared to control littermates, deletion of *Vps13c* had little effect on
31 glucose tolerance. Pancreatic histology revealed no significant change in β cell mass in KO mice
32 *versus* controls and glucose-stimulated insulin secretion from isolated islets was not altered *in vitro*
33 between control and β *Vps13c*KO mice. However, a tendency was observed in female null mice for
34 lower insulin levels and β cell function (HOMA-B) *in vivo*. Furthermore, glucose-stimulated increases
35 in intracellular free Ca^{2+} were significantly increased in islets from female KO mice, suggesting
36 impaired Ca^{2+} sensitivity of the secretory machinery. The present data thus provide evidence for a
37 limited role for changes in *VPS13C* expression in conferring altered disease risk at this locus,
38 particularly in females, and suggest that *C2CD4A* may also be involved.

39

40 **Key words**

41 VPS13C, C2CD4A, GWAS, type 2 diabetes, β cell.

42

43

44

45 **Introduction**

46

47 The incidence of Type 2 diabetes (T2D) is now reaching epidemic proportions across the globe, with
48 deaths from the disease reaching 5.1 million and disease complications costing USD 548 billion in
49 2013 (30). These values are expected to continue to increase, with predictions of a further 205 million
50 sufferers by 2035 (30). T2D is a complex metabolic disease involving hyperglycaemia and
51 dyslipidemia, which together conspire to cause serious secondary macro-and microvascular
52 complications including cardiovascular disease, retinopathy and neuropathy (11, 19). Although it is
53 accepted that a loss of an appropriate balance between functioning pancreatic β cell mass, and insulin
54 action in peripheral tissues, lead to abnormal glucose homeostasis, the molecular basis of T2D onset
55 and progression are still poorly understood (31, 57).

56 Whilst environmental factors such as increasingly sedentary lifestyles and obesogenic diets have a
57 substantial impact, genetic susceptibility also plays a significant role in T2D risk (57).
58 Correspondingly, Genome-Wide Association Studies (GWAS) have identified ~90 *loci* harbouring
59 single nucleotide polymorphisms (SNPs) that confer increased disease risk (13, 21, 23, 40, 57, 65,
60 86). Such studies have thus led to the discovery of novel genes involved in T2D, such as T-cell factor
61 7-like 2 (*TCF7L2*) (21) and *SLC30A8* (58, 65). Of note, the majority of the GWAS-identified *loci*
62 affect insulin secretion rather than action, further emphasising the likely role in disease aetiology of
63 impaired insulin production.

64 The *VPS13C/C2CD4A/C2CD4B* locus was first associated with T2D and glycaemic traits in GWAS
65 published in 2010 (6, 15, 22, 29, 60). Subsequent studies identified further SNPs at this genomic
66 location associated with poorer glycaemic control and T2D (12, 67, 78). The above studies
67 encompassed a range of distinct populations and age groups thus providing confidence that SNPs in
68 this *locus*, acting either via nearby or more remotely located genes, alter genetic susceptibility to T2D.
69 SNPs within the *VPS13C/C2CD4A/B* locus have been linked to a range of glycaemic parameters
70 including higher fasting proinsulin (29, 67), higher 2 h glucose and lower 2 h insulin (60, 67), as well
71 as increased fasting glucose (15, 22, 67) and increased waist circumference (22). Two studies also

72 associated risk alleles with lower glucose stimulated insulin secretion (GSIS; (6, 22, 67)) and others
73 with T2D (12, 67, 83). The ‘lead’ (GWAS index) SNP in this *locus*, rs7172432, is in LD with a
74 ‘functional’ SNP, rs7163757, previously implicated by fine mapping as the most strongly associated
75 ($p=3\times 10^{-19}$) SNP at this *locus* (61, 66). rs7163757 is located in an islet stretch enhancer (50, 61, 66),
76 again suggesting that the disease-associated SNP acts on the expression of an effector gene(s) to alter
77 diabetes risk.

78 The first identified member of the highly conserved VPS13 family of proteins was *Soi1* (or *Vps13*) in
79 *S. cerevisiae* where it plays an important role in membrane protein trafficking between the trans-Golgi
80 network (TGN) and the prevacuolar compartment (7). Specifically, *Vps13* is involved in trafficking
81 the protease *Kex2p*, a protein involved in intracellular insulin processing after over-expression of the
82 latter in yeast (85). Subsequently, a role for this protein was demonstrated in prospore formation in *S.*
83 *cerevisiae* through the regulation of phosphatidylinositol-4-phosphate (PI(4)P) generation and
84 membrane-bending activity (48, 49).

85 In both humans and mice, the VPS13 family comprises four members (A-D) with VPS13A and C
86 showing the most similarity to the yeast homologue (73). All four proteins are large proteins which
87 have potential functions in membrane protein trafficking, Golgi structure and/or phosphatidylinositol
88 metabolism (37, 47, 53, 62, 63, 73). Mutations in *VPS13A* and *VPS13B* cause the genetic diseases
89 Chorea-Acanthocytosis and Cohen syndrome, respectively (32, 53, 71) and a loss of VPS13C function
90 has recently been linked to early-onset Parkinson’s disease (35).

91 VPS13C is ubiquitously expressed in mammals, with particularly high levels in pancreatic islets and β
92 cells (60, 67). The above observations have thus led us to hypothesise that VPS13C may play a role in
93 the intracellular trafficking of insulin or other aspects of pancreatic β cell function. To explore this
94 possibility, we have first determined the relationship between the possession of T2D risk alleles in
95 man, and the expression of *VPS13C*, *C2CD4A* and *C2CD4B* in human islets. Subsequently, we have
96 developed mice inactivated for *Vps13c* highly selectively in the β cell using the recently-developed
97 *Ins1Cre* deleter strain (33, 69). The latter is a knock-in model which avoids the complications

98 associated with earlier insulin 2 promoter-dependent *Cres* including recombination in the brain (77)
99 and co-expression of human growth hormone (8). This approach reveals roles for *Vps13c* in the
100 control of whole body glucose homeostasis, insulin secretion *in vivo* and glucose-induced Ca^{2+} signal
101 generation in the β cell, but suggests that *C2CD4A* may also contribute to disease risk.

102

103

104 **Materials and Methods**

105 *Materials*

106 All general chemicals and materials were purchased from Sigma (Dorset, UK) or Fisher Scientific
107 (Loughborough, UK) unless indicated.

108 *Generation of VPS13C antibodies*

109 A custom polyclonal antibody against human VPS13C, based on amino acids 1582-1882 of human
110 VPS13C isoform 2A (UniProtKB Q709C8-1; 84% identities, 92% positives with mouse VPS13C
111 protein Q8BX70-1, positions 1580-1879) was raised in rabbits as recently described (84).

112 *Ethics*

113 All *in vivo* procedures were conducted in accordance with U.K. Home Office regulations (Animals
114 (Scientific Procedures) Act of 1986, Home Office Project License number PPL 70/7349, Dr Isabelle
115 Leclerc). Procedures were performed at the Central Biomedical Service at Imperial College, London.
116 Isolation of islets from multi-organ donors was approved by the local ethical committee at the
117 University of Pisa. Human pancreata were collected from brain-dead organ donors after informed
118 consent was obtained in writing from family members. Use of human islets at Imperial College was
119 approved by the local NRES Committee, Fulham; REC reference 07/H0711/114.

120 *eQTL analysis*

121 Human islet DNA samples obtained from 53 donors (see *Supplementary Table 1* for clinical
122 characteristics), using the DNeasy Blood & Tissue Kit (Qiagen, Hilden, Germany) as previously
123 described (51), were genotyped for SNPs rs4502156, rs7172432 and rs7163757. The rs7172432 locus
124 was amplified by semi-nested PCR using primers TAG GTA TCT TGG AGC TGA GG and CCA
125 CAC TTC ACA GAA TCA GG for the first round amplification then CAG GTC AAG TGA GCA
126 CTT GC and CCA CAC TTC ACA GAA TCA GG for the second round. The amplicons were then
127 digested with *SspI* and genotyped based on the resulting restriction fragment length polymorphism.

Islet RNA was isolated from hand-picked islets as described (39), using the Arcturus PicoPure RNA Isolation Kit (Applied Biosystems, Foster City, CA), according to the procedure recommended by the manufacturer for RNA extraction from cell pellets, and, accordingly, was treated with DNase to remove the contamination with genomic DNA. Reverse transcription to cDNA was performed using a High Capacity cDNA Reverse Transcription Kit (ThermoFisher). The rs4502156 and rs7163757 SNPs were genotyped by qPCR using a commercial TaqMan assay (Applied Biosystems). *VPSI3C*, *C2CD4A* and *C2CD4B* mRNA abundances were measured relative to *ACTB* in corresponding RNA samples by qRT-PCR using commercial TaqMan assays (Applied Biosystems) and the ΔC_t method. As a quality control step, samples with ΔC_t standard deviation > 0.2 were excluded from the analysis. The association between *VPSI3C* expression and genotype was tested using an ANCOVA model, controlling for age, gender and BMI and implemented in R (52). The association of genotype with *C2CD4A* and *C2CD4B* was analysed in the same manner. Linkage disequilibrium (LD) values for SNPs in the Tuscan population used here were obtained at: <http://www.1000genomes.org/faq/which-populations-are-part-your-study>.

Luciferase construct cloning and assay

To assess whether variants at rs7163757 might cause changes in the expression of nearby genes, two reporter constructs were generated. A 1.3kb fragment of the genomic region flanking the SNP was amplified by PCR from a heterozygous donor using Phusion High Fidelity DNA Polymerase (Thermo Scientific, Paisley, UK). The PCR product was subsequently cloned into CRTM8/GW/TOPO (ThermoFisher, Paisley, UK) according to manufacturer's instructions. Plasmid DNA from clones was purified using GenEluteTM Plasmid Miniprep Kit (Sigma, Dorset, UK) and sent for sequencing to identify clones containing one of each allele. DNA fragments were then shuttled into the minimal promoter (DNA Sequence: TAG AGG GTA TAT AAT GGA AGC TCG ACT TCC AG, containing a TATA-box promoter element)-driven luciferase vector GL4.23-GW vector (76) using Gateway LR Clonase II Enzyme Mix (Invitrogen, Paisley, UK). pGL4.23-GW is modified from pGL4.32 (Promega) with Gateway^R technology (ThermoFisher) and has previously been used successfully for the analysis of enhancer activity (20).

155

156 The sequence and orientation of the insert was checked by restriction enzyme digest and subsequently
157 a QIAGEN Plasmid Maxi Kit (QIAGEN Ltd, Manchester, UK) was used to purify transfection grade
158 DNA. HEK293, MIN6 (44), 1.1B4 (41) and EndoC- β H1 (54) were transfected using Lipofectamine
159 2000 (Invitrogen, Paisley, UK) in 48 well plates using 250 ng of each reporter construct and 1 ng of
160 *Renilla* control vector. Each condition was repeated in six separate wells. Dual-Luciferase Reporter
161 Assay (Promega, Southampton, UK) was used to measure Luciferase normalised against Renilla. All
162 experiments were done in triplicate. The following cloning primers were used: CCA ACA AAT AGT
163 AAG CAT TAT TAC C (rs7163757, forward) and CAA ATA GTT GTA GAT ATG TGG CAT T
164 (rs7163757, reverse).

165 *Mouse generation, housing and genotyping.*

166 Generation of heterozygous embryos on a C57/BL6 background, carrying floxed alleles of *Vps13c*
167 was conducted by GenOway (France). *Vps13c*^{fl/fl} mice were crossed to mice expressing *Cre*
168 recombinase under the control of the Ins1 promoter (33, 69) to generate mice in which exon 1 of the
169 *Vps13c* gene was selectively excised in pancreatic β cells. Mice were born at the expected Mendelian
170 ratios without any obvious physical or behavioural defects. Mice were housed 2-5 per cage in a
171 pathogen-free facility under a 12-hour light and dark cycle and had *ad libitum* access to water and
172 standard mouse chow diet (Research Diet, New Brunswick, NJ, USA). High fat diet (HFD, 60%
173 [wt/wt] fat content; Research Diet, New Brunswick, NJ, USA) was introduced at four weeks of age.

174 Genotyping was performed from ear biopsies using PCR. Knockout of *Vps13c* from pancreatic islets
175 was assessed using both qPCR and immunoblotting as described below. Mice were weighed weekly
176 from five weeks of age and random, fed glycaemia was tested fortnightly in the afternoon.

177 *Intraperitoneal (IP-) and oral (O-) glucose tolerance tests (GTTs)*

178 Mice were fasted for 15-16 hours overnight prior to IP- or OGTT with free access to water. Blood
179 samples were taken for glycaemia measurement via venesection of the tail vein. Glycaemia was

measured using an Accu-Chek[®] glucometer (Roche Diabetes Care Ltd, UK) and appropriate measurement strips. Fasting glycaemia was first measured (time 0) and then glucose was administered via IP injection (1 g/kg body weight) or oral gavage (1.5 g/kg body weight). Glycaemia measurements were then taken at 15, 30, 45, 60, 90 and 120 min. post injection.

Measurement of plasma insulin and proinsulin

Mice were fasted overnight with free access to water. A fasting (time 0) blood sample (~50 µl) was collected from the tail vein into a lithium-heparin lined-Microvette[®] (Starstedt, Leicester, UK) before administering glucose (3 g/kg body weight) via IP injection. Blood samples were then collected at 15 and 30 min. after injection. Glycaemia was also measured at these time points. Plasma was collected by centrifuging samples at 2000 *g* for 10 min. at 4°C. Plasma insulin was measured using an ultrasensitive mouse insulin ELISA (Crystal Chem, IL, USA). For random-fed insulin/proinsulin ratio measurements, a blood sample was collected into a lithium-heparin lined Microvette[®] from the tail vein and the aorta immediately after culling via cervical dislocation. Samples were kept on ice at all times to prevent degradation of proinsulin and plasma was collected as described above. Insulin was measured as described above and proinsulin was measured using a Rat/Mouse Proinsulin ELISA (Mercodia, Uppsala, Sweden).

Homeostatic model (HOMA) analysis

HOMA2-%S and-%B (36) were calculated using fasting glycaemia and plasma insulin measurements, with the HOMA Calculator[™], as described: <https://www.dtu.ox.ac.uk/homacalculator/download.php>

Isolation of islets and assay of insulin secretion

Mice were culled by cervical dislocation. Islets were isolated after pancreatic distension with collagenase essentially as previously described (55). Islets were allowed to recover from digestion for 24 (RC-fed mice) or 48 (HFD-fed mice) h in RPMI medium (Gibco) supplemented with 10% (v/v) foetal bovine serum, 1% (w/v) Penicillin, 1% (w/v) Streptomycin, 11.1 mM glucose and 2 mM L-glutamine. Insulin secretion was measured from duplicate batches of 10 islets incubated in 0.5 ml of

205 Kreb's-Ringer medium (130 mM NaCl, 3.6 mM KCl, 1.5 mM CaCl₂, 0.5 mM MgSO₄, 0.5 mM
206 NaH₂PO₄, 2 mM NaHCO₃, 10 mM HEPES, and 0.1 % [w/v] bovine serum albumin (BSA), pH 7.4)
207 containing 3 mM or 16.7 mM glucose, or 20 mM KCl and 3 mM glucose as indicated, shaking at
208 37°C for 30 min. Total insulin was extracted into 0.5 ml acidified ethanol (75% [v/v] ethanol, 1.5%
209 [v/v] 1M HCl and 0.1% [v/v] Triton X-100). For continuous measurements of secretion, insulin
210 samples from 50 perfused islets were collected using a custom-built device, using a perfusion rate of
211 500 µl/min at 37°C as described previously (10). Secreted and total insulin concentrations were
212 measured using a homogeneous time-resolved fluorescence-based (HTRF) insulin assay (CisBio,
213 Codolet, France) in a PHERAstar reader (BMG Labtech), according to manufacturer's instructions.

214 *Determination of β and α cell mass*

215 Isolated pancreata were fixed in 10% (v/v) formalin overnight at 4°C and embedded in paraffin wax.
216 Sections (5 µm) were cut and fixed onto Superfrost slides. For staining, five sections per mouse, 25
217 µm apart, were incubated in Histochoice[®] Clearing Agent and then submerged consecutively in 100%,
218 95% and 70% ethanol to remove the wax. Following washes with water, sections were permeabilised
219 by boiling in a citrate-based antigen unmasking solution (Vector Labs, Peterborough, UK), washed
220 with PBS and then incubated in PBS-Triton X-100 (PBST, 0.1% [v/v]) containing 2% (w/v) BSA and
221 2% (v/v) goat and donkey serum for 2 h at room temperature. Sections were then incubated in a
222 humidified chamber at 4°C overnight with guinea-pig anti-insulin (1:200; Dako, Ely, UK) and mouse
223 anti-glucagon (1:1000; Sigma, Dorset, UK). After washing three times in PBST (0.25% [v/v])
224 containing 0.25% (w/v) BSA, sections were incubated with Alexa fluor-488 and -568 conjugated
225 secondary antibodies (1:1000; Invitrogen, Paisley, UK) for 2 h at room temperature in the dark.
226 Sections were then mounted using Vectashield antifade mounting medium containing DAPI (Vector
227 Labs, Peterborough, UK). Slices were imaged in the Imperial College facility for imaging by light
228 microscopy (FILM) (<http://www3.imperial.ac.uk/imagingfacility>), using a Zeiss Axio Observer
229 inverted widefield microscope with LED illumination. Images were captured with a Hamamatsu Flash
230 4.0 fast camera controlled by Zen software (Zeiss, Cambridge, UK). Image analysis was conducted
231 using ImageJ software (1) and an in-house macro as described under *Supplementary Methods*.

232 *Quantitative real-time PCR (qPCR) analysis*

233 Total RNA was extracted from (50-200) islets isolated from three control and three $\beta Vps13c$ KO mice
234 (for both males and females) using TRIzol (ThermoFisher Scientific), according to the manufacturer's
235 instructions. RNA (100 ng) was reverse transcribed to produce cDNA using the High Capacity
236 Reverse Transcription Kit (Life Technologies, Paisley, UK) with random primers. qPCR was
237 conducted using SYBER Green (life Technologies, Paisley, UK) on a ABI-Fast Prism 7500 machine
238 and primers specific to murine *Vps13c*, *C2cd4a*, *C2cd4b* or *CyclophilinA*. Primers were designed
239 using Primer Express 3.0 (Applied Biosystems, CA, USA) and sequences used were: *Vps13c*
240 (forward) CAC AAG CAT TGA AGA TAG AAG CAA AA; *Vps13c* (reverse) AGT GAT GGC
241 ACA ATG TCT TGT TG; *C2cd4a* (forward) CGG GTT GGA AAA CCA TCT GA; *C2cd4a* (reverse)
242 GTC TGA ACC CTG TGA TCC TGT TC; *C2cd4b* (forward) ACG TCA CCT GCT TCG TTC CT;
243 *C2cd4b* (reverse) CAC GAG CGT CTT TTC TTC TTC A; *CyclophilinA* (forward) TAT CTG CAC
244 TGC CAA GAC TG A; *CyclophilinA* (reverse) CCA CAA TGC TCA TGC CTT CTT TCA. Whereas
245 the *VPS13C* and *C2CD4B* primers spanned exon/exon junctions, the *C2CD4A* primers spanned intron
246 1.

247 *Western (immuno-) blotting*

248 Total protein was extracted from 50-500 islets isolated from 2-3 control or $\beta Vps13c$ KO mice (males
249 and females) in ice-cold RIPA buffer (1% [v/v] Triton X-100, 1% [w/v] sodium deoxycholate, 0.1%
250 [w/v] SDS, 0.15 M NaCl, 50 mM Tris, pH 8.0) containing a 2x concentration of cOmplete, EDTA-
251 free protease inhibitor cocktail (Roche, Burgess Hill, UK). The samples were incubated in RIPA on
252 ice for 10 min. and then freeze-thawed twice to ensure release of proteins. Samples were clarified by
253 centrifuging at 16,000 g for 10 min. at 4°C and then total protein content was quantified using a BCA
254 protein assay kit (Pierce, ThermoScientific). 5 µg total protein was added to SDS sample buffer (0.5
255 M Tris-HCl, pH 6.8, 2% [w/v] SDS, 5% [w/v] glycerol, 0.6 M DTT and 0.2 mg bromophenol blue)
256 and incubated at room temperature for 30 min. Samples were then electrophoresed on a 4-10%
257 discontinuous gradient gel alongside a HiMark Protein Standard (Novex®, ThermoScientific) and

transferred onto a nitrocellulose membrane overnight. Membranes were blocked with 5% milk and incubated with primary antibodies (rabbit anti-VPS13C, 1:2000, described above) or goat anti-EEA1, Santa Cruz, Texas, USA, 1:2000) overnight with agitation at 4°C. Membranes were then washed three times in PBS-Tween20 (0.2%[v/v]) and incubated with horseradish peroxidase-conjugated antibodies for 1 h at room temperature. Following three washes in PBS-Tween20, proteins were visualised with ECL reagent and x-ray film (Amersham, GE Healthcare Life Sciences).

Confocal immunocytochemistry

Human islets were dissociated by 10 min. incubation in Hanks' based enzyme-free cell dissociation buffer (GIBCO, Invitrogen) and gentle pipetting to generate small clusters of cells. Dissociated cells were plated onto 13/24 mm sterile coverslips and allowed to recover for 1-2 days. Cells were fixed in 4% paraformaldehyde and permeabilized in 0.1% Triton X 100. Primary cells were blocked in 10% foetal calf serum and subsequently incubated overnight with VPS13C 15-E antibody (Santa Cruz sc-104751, 1:50) with or without anti-insulin antibody (1:200; Dako, Ely, UK) followed by incubations with Alexa-488 and Alexa-568-conjugated secondary antibodies in sequential order. Coverslips were mounted using VectaShield with DAPI and imaged as described elsewhere (42). Samples were illuminated using steady state 488 and 560 nm laser lines and emission was collected through ET535/30 and ET620/60 emission filters (Chroma). Images were captured using a Hamamatsu EM CCD Digital camera controlled by an Improvision/Nokigawa spinning disc system running Volocity™ (PerkinElmer, MA, USA) software.

Confocal Ca²⁺ imaging

Islets were isolated as described above. Simultaneous imaging of Ca²⁺ of individual cells was performed by spinning disc confocal microscopy after loading intact islets with Fluo-2 AM (Cambridge Bioscience, Cambridge, UK). Images were captured with a Zeiss Axiovert 200M microscope fitted with a 10x 0.3-0.5 NA, EC Plan Neofluar, Zeiss objective and a 1.5x Optivar attached to a Nokigawa spinning disc confocal head, as described (27). The microscope was controlled using Volocity™ software. Islets were continuously perfused in KREB's-Ringer buffer

containing 3 mM glucose, equilibrated with 95% O₂/5% CO₂ at 34-36°C. Islets were stimulated at 210 s and 1300 s by perfusion with KREB's-Ringer supplemented with up to 16.7 mM glucose or 20 mM KCl as indicated. Offline processing and analysis were conducted using ImageJ software (1) and an in-house macro as described under *Supplementary Methods*.

Statistics

Data were analysed using Microsoft Excel, GraphPad PRISM 6.0 and R. Significance was tested using unpaired Student's two-tailed t-test with appropriate post-tests for multiple comparisons, or two-way ANOVA, as indicated. P<0.05 was considered significant and errors signify means ± SEM unless stated. Figures were constructed using Adobe Illustrator.

Results

eQTL analysis

GWAS studies have implicated SNPs close to *VPSI3C*, *C2CD4A* and *C2CD4B* in altered T2D susceptibility. We tested the association between genotype at one of the previously-identified SNPs rs4502156 and the likely causal SNP rs7163757 (61, 66) ($r^2=0.939$, $D'=0.979$ with rs4502156) and *VPSI3C* expression in human islet samples from 53 donors. Initial analysis for rs4502156 and rs7163757 including all samples showed no significant association. Interaction plots indicated a possible interaction between gender and genotype which was tested by including the interaction term in the ANCOVA model (See Methods). This was found to be significant ($p=0.015$, $n=53$) so data were stratified by gender and subsequently males and females were analysed separately (Fig. 1A-C). Analysis of females revealed a significant association between possession of the risk allele (C) at rs7163757 and lowered *VPSI3C* expression ($p=0.041$, $n=40$, Fig 1C). A similar gender interaction ($p=0.016$, $n=53$) was also observed for rs4502156, and likewise a significant association was detected between genotype at this locus and expression of *VPSI3C* in females ($p=0.043$, $n=40$). An association was also detected between rs4502156 (not shown), as well as rs7163757 ($p=0.011$, $n=40$, Fig. 1 D-F),

with *C2CD4A* mRNA levels in female donors, but not with *C2CD4B* (Fig 1G-I). Subsequent functional studies in the present report focussed upon *VPSI3C*.

Impact of risk alleles on enhancer activity assessed by reporter luciferase assay

To determine whether and how the possession of risk alleles at the *VPSI3C* locus might affect the expression of nearby or remotely-located genes, we used reporter-luciferase assays in non- β -cells (HEK293) and in β cell lines from mouse (MIN6) and human (1.1B4 and EndoC β H1). As shown in Fig. 2, inclusion of the risk (C) allele at the previously-implicated causal SNP rs7163757 significantly lowered the enhancer/promoter activity of reporter constructs bearing this variant *versus* the presence of the protective (T) allele in HEK293, MIN6 and 1.1B4 cells. A similar tendency ($p < 0.1$) was observed in EndoC β H1 cells (Fig. 2). These data are thus consistent with an enhancer function for this region, whose activity is lowered in carriers of risk alleles.

*Impact of β -cell-selective deletion of *Vps13c* on body mass and fasting glycemia*

The above observations suggested that risk variants at the *VPSI3C* locus may decrease the expression of nearby genes. To explore the potential impact of lowered *VPSI3C* levels on insulin secretion, deletion of exon 1 (Fig. 3A) of the *Vps13c* gene was achieved throughout the pancreatic β -cell compartment in C57BL/6 mice from \sim E11.5 using the highly selective *Ins1 Cre* deleter strain (69). As shown in Figs 3B and 3C, *VPSI3C* was barely detected in islets isolated from β *Vps13c*KO mice (Fig. 3B and C (i)) and levels of *Vps13c* mRNA were significantly reduced (Fig. 3B(ii) and C(ii)) by $>80\%$. These findings are fully consistent with efficient ($>94\%$) and exclusive (69) recombination in β cells, which comprise 60-80% of the rodent islet (16) given that *Vps13c* mRNA is ~ 2 -fold more abundant in β than in α cells (5), which comprise the majority of the islet non- β cells. Expression of *C2cd4a* and *C2cd4b* in islets was variable between mice but was unaffected by *Vps13c* deletion. Changes in body weight gain (Fig. 3D, E) and random fed glycaemia (Fig. 3F, G) over time were not different between control (Ctrl) and β *Vps13c*KO mice, irrespective of gender or diet (regular chow [RC] *versus* high fat diet [HFD]; see Materials and Methods for details).

*β *Vps13c*KO mice display age-dependent abnormalities in glucose tolerance*

Examined in male mice, intraperitoneal glucose tolerance (IPGTT) was not different between control and $\beta Vps13c$ KO animals up to the age of 16 weeks, whereas $\beta Vps13c$ KO mice became glucose intolerant at 20 weeks of age (Fig. 4 A, C, E, G). Although glucose tolerance was lower at all ages examined compared to animals maintained on RC, no differences were observed between control and $\beta Vps13c$ KO males maintained for up to 16 weeks (i.e., 20 weeks old) on a HFD (Fig. 4 B, D, F, H).

By contrast, when maintained on RC, female mice (Fig. 5) displayed abnormal IPGTT at 12 weeks of age (Fig. 5C). This resolved at 16 weeks but was again apparent at 20 weeks (Fig. 5G). Consistent with observations in males (Fig. 4), female $\beta Vps13c$ KO mice fed HFD similarly failed to show abnormalities in IPGTT up to 20 weeks of age (Fig. 5, B, D, F, H).

To test a possible role for $Vps13c$ in responses to incretin hormones, we next performed oral glucose tolerance tests (OGTT) in RC-fed mice. No genotype-dependent differences were apparent in males (Fig. 6A) or females (Fig. 6B) examined at 22 - 24 weeks.

Examined in mice aged 19-21 weeks, glucose-induced excursions in plasma insulin were not different between $\beta Vps13c$ KO and control male and female mice (Fig. 7A-D). Likewise, by analysing fasting glucose and insulin levels, we observed no indication of a change in steady state β cell function (36) as assessed using homeostatic model assessment (HOMA2-%B; Fig. 7E), nor insulin in insulin sensitivity (HOMA2-%S; Fig. 7F) in males maintained on either RC or HFD. By contrast a tendency towards a lower HOMA2-%B value (Fig. 7G), accompanied by a significant increase in HOMA2-%S, was apparent in female $\beta Vps13c$ KO mice *versus* controls fed on RC, whilst these differences were not observed on HFD (Fig. 7 G, H).

Impact of $Vps13c$ deletion on glucose-and KCl-stimulated insulin secretion in vitro

Impairments in glucose tolerance and a tendency towards impaired β cell function apparent *in vivo* in female $\beta Vps13c$ KO mice might reflect abnormal glucose- or depolarisation-dependent insulin secretion from β cells. To investigate this, we studied insulin release from batches of islets from mice 20-23 weeks old as shown in Fig. 8. Interestingly, both glucose- (16.7 mM) and KCl- (20 mM) stimulated secretion tended to increase in $\beta Vps13c$ KO *versus* control islets from males fed either RC

(Fig. 8A) or HFD (Fig. 8B). Whereas a similar tendency was also apparent for islets from females maintained on a HFD (Fig. 8D), those from female $\beta Vps13c$ KO mice fed RC showed no change in insulin secretion *versus* controls (Fig. 8C) when stimulated with 20 mM KCl. No differences between HFD-fed control and $\beta Vps13c$ KO mice were seen when the same experiment was conducted under perfusion (Fig. 8E).

β cell mass is not changed after $Vps13c$ deletion.

One explanation for the differences in glucose tolerance and insulin secretion seen in $\beta Vps13c$ KO mice may be an alteration in β cell mass. To establish whether this was the case, we conducted immunohistochemical analyses on pancreatic sections from $\beta Vps13c$ KO and control mice fed RC and aged over 20 weeks. Using antibodies against either insulin or glucagon we observed no differences in % β or α cell surface normalised pancreatic surface (Fig. 9A and B, females; C and D, males).

Gender-specific effects of $Vps13c$ deletion on intracellular Ca^{2+} dynamics.

Alterations in glucose tolerance and tendency towards impaired insulin secretion, which were apparent *in vivo*, may reflect altered signal generation by glucose. We next used the fluorescent intracellular probe Fluo-2 (27) to monitor intracellular free Ca^{2+} dynamics in β cells *in situ* within the intact islet (Figs 10, 11). Under the conditions used, glucose-induced changes in free Ca^{2+} are largely restricted to the β cell population (10, 27). No genotype-dependent differences in the peak of the Ca^{2+} response to either high glucose or KCl were apparent in islets from male mice (Fig. 10) although islets from male $\beta Vps13c$ KO mice fed RC did display a significantly delayed response to high glucose stimulation (Fig. 10A(ii) and (v)). Increases in free Ca^{2+} in islets from female mice were respectively augmented (Fig. 11A (i) and (vi)) and reduced (Fig. 11B (i) and (vi)) in high glucose-stimulated islets from $\beta Vps13c$ KO animals fed RC or HFD. A similar trend was seen after depolarisation with KCl (Figs. 11A (i) and (viii) and B (i), (iv) and (viii)). As was the case for male mice, the response to glucose in islets from HFD-fed female mice was slightly delayed, with those from RC mice showing no significant difference in the time of the glucose peak (Fig. 11A (i) and (v) and B (i) and (v)).

Subcellular localisation of VPS13C in human β cells

387 To determine whether VPS13C might conceivably affect the properties (i.e “fusogenicity”), or the
388 distribution of secretory granules, we explored the localisation of the protein with single human β
389 cells by confocal immunocytochemistry (Fig. 12). Close co-localisation was observed between insulin
390 and VPS13C-labelled structures, indicative of the presence of the latter on the limiting membrane of
391 insulin-containing dense core granules.

392

393 Discussion

394 Previous studies (17) have revealed that *VPSI3C* expression in human islets is associated with HbA1c
395 levels by massive parallel sequencing (RNA-seq) and microarray analysis at both nominal and
396 permutation p-values ($p < 0.05$), with lower mRNA levels observed in T2D subjects. We extend these
397 findings here by showing that *VPSI3C* mRNA levels are lower in carriers of risk alleles at rs4502156
398 and rs7163757 in female, but not male subjects. We note that in the present study a lower number of
399 male *versus* female samples may have limited our power to detect changes in the former. However,
400 and arguing against this possibility, no tendency towards lowered *VPSI3C* or *C2CD4A* expression
401 with the interrogated SNPs was observed in males: rather, the trend was towards increased expression
402 with risk alleles.

403 Using mouse genetics we provide evidence that *VPSI3C* plays a role in the control of pancreatic β cell
404 function. It should be emphasised that the impact of deleting this gene selectively in the β cell was
405 relatively mild, and indeed was not apparent in males until 20 week of age. Evidence for deficiencies
406 in β cell function were, however, more apparent in females from an earlier age, in line with the human
407 eQTL data. These included the transient appearance of glucose intolerance at 12 weeks and its re-
408 emergence at 20 weeks. Interestingly, the same phenomenon is also observed in a monogenic form of
409 diabetes resulting from mis-expression of the *ZAC* gene, termed transient neonatal diabetes mellitus
410 (TNDM), and is apparent in mouse models this disease (albeit in younger animals than observed here)
411 (38). Whilst the reasons for this transience are not known either in TNDM nor in the case of *Vps13c*
412 deletion, dynamic changes in the balance between islet function and insulin sensitivity may provide
413 one explanation. Similarly, the (monophasic) emergence of glucose intolerance with age in
414 $\beta Vps13cKO$ mice, which is reminiscent of changes seen after the inactivation of the T2D GWAS gene
415 *Tcf7l2* in mice (43, 82), seems to reflect, at least in part, increasing insulin resistance, as well as
416 impaired insulin output from the pancreas. Of note, recent studies report relatively preserved glucose
417 sensing of isolated islets with age in both mice and humans (3, 26), but suggest a role for altered
418 vascularisation and fibrosis in impaired insulin secretion *in vivo* (3).

Strikingly, impairments in glucose tolerance apparent in both male and female $\beta Vps13c$ KO mice *versus* littermate controls at this age were abolished after maintenance on HFD. These findings demonstrate an interesting interaction between the inheritance of a genetic factor influencing risk, and age (as observed in human T2D, (87)) as well as sex and diet. The reasons for the difference in penetrance between the effects of $Vps13c$ deletion observed here between male and female mice remain unknown but may reflect interactions with sex hormones at the level of the individual β cell (46), or alternatively, subtle differences in insulin sensitivity between the sexes which go on to influence the effect of perturbations in the β cell on overall glucose homeostasis.

Examined in either males or females, β cell mass was not different between control and knockout mice, indicating a possible defect in β cell function as underlying the glucose dyshomeostasis reported above. Correspondingly, clear tendencies were apparent towards impaired β cell function and lowered insulin levels when combining fasting glycaemia with corresponding insulin plasma concentration using HOMA2 analysis (particularly in females (Fig. 7E, G). According to this analysis, insulin sensitivity was slightly but significantly increased in knockout females *versus* littermate controls (Fig. 7H), again indicating that a defect in β cell function is likely to underlie the mild glucose intolerance in knockout mice (and subject to caveats in extrapolating HOMA2 models from humans to rodents) (74).

On the other hand, we were unable to detect any impairment in glucose or depolarisation-induced insulin secretion as assessed *ex vivo* in isolated islets (Fig. 8). Indeed, in islets isolated from animals maintained on either RC or HFD we observed a tendency in male $\beta Vps13c$ KO mice towards enhanced insulin secretion in response to either high glucose or KCl and in female $\beta Vps13c$ KO in response to high glucose. By contrast, stimulated insulin secretion in response to KCl tended not to change in $\beta Vps13c$ KO *versus* control islets from females fed RC, or HFD. We are therefore unable at the present time to assign the changes in β cell function and glucose homeostasis observed *in vivo* unambiguously to alterations in islet responses measurable *in vitro*. We would stress, however, that the mechanisms responsible for the stimulation of insulin secretion by elevated glucose *in vivo*, which

are likely to be modulated by a multitude of humoral (e.g. circulating fatty acids, incretins, adipokines etc), neuronal (56) and other inputs into the islet, are unlikely to match perfectly those tested *in vitro*.

Nonetheless, detailed analysis of glucose- and KCl-induced Ca^{2+} dynamics did provide evidence for alterations at the level of secretory granule behaviour, which may play a role to impair insulin secretion *in vivo*. Importantly, islets from male $\beta Vps13c$ KO mice maintained on regular chow or on HFD responded normally with insulin secretion in response to either glucose or high KCl (Fig. 8), consistent with mild, and late onset, glucose intolerance in these animals. Glucose-induced Ca^{2+} increases were nonetheless significantly delayed in the KO animals (Fig. 10). By contrast, when fed on regular chow, islets from female $\beta Vps13c$ KO mice displayed a significant enhancement in glucose-stimulated Ca^{2+} increases *versus* islets from control littermates (Fig. 11A), whilst GSIS was unaltered (and tended to be decreased in response to KCl), as mentioned above. These observations suggest that the Ca^{2+} -responsiveness of the secretory machinery to intracellular Ca^{2+} increases may be diminished in female $\beta Vps13c$ KO mice, perhaps reflecting changes in the number of fusion-competent secretory granules, as reported after manipulation of the GWAS gene *TCF7L2* (81) or the microRNA miR124 (4) and might suggest a common mode of action of genes affecting T2D risk. Finally, it is possible, given that proinsulin levels were elevated in carriers of risk alleles, that prohormone processing is altered after *Vps13c* inactivation (67). To investigate this hypothesis, we measured random-fed insulin and proinsulin concentrations in RC-fed mice. No differences were seen in either insulin or proinsulin plasma concentrations, nor was the insulin/proinsulin ratio different between controls and KO mice (results not shown).

Changes in glucose tolerance were not apparent after the maintenance of mice (either male or female) on a high fat diet, suggesting that the phenotype might be rescued by changes in response to high fat feeding and insulin resistance. One possible explanation might be an increase in the expression of other VPS13 family members, which could be triggered by a HFD, thus compensating for the absence of VPS13C. According to a recent study of mouse islet cell transcriptomes (5), *Vps13c* mRNA levels are 2-3 times those of *Vps13a*, *-b* and *-d* in the β cell under conditions of normal feeding. Whether changes in the expression of any of these genes occur under the stress of a high fat diet has yet to be

investigated. We note also that a recent eQTL study (9) did not report a significant association with *VPS13C* (or other genes at this locus) and T2D risk, though whether the latter study was adequately powered to detect small changes is uncertain.

How might VPS13C influence insulin secretion *in vivo*? Clues might be gleaned by comparisons with other members of the VPS13 family. BLAST analysis of the protein sequences of the four family members indicates that VPS13C is most similar to VPS13A, sharing 41% identity (73) and the two proteins possess several common domains and have similar N- and C-termini, indicating that they may have similar functions (73). Both can attach to membranes, although VPS13C has intramolecular duplications *versus* VPS13A, which may imply neofunctionalisation (i.e. the acquirement of new roles) compared to VPS13A (73). A loss of VPS13A (also called chorein) expression leads to the rare neurodegenerative disease Chorea-Acanthocytosis (ChAc) (53, 71). Symptoms include cognitive dysfunction, hyperkinetic movement disorder and erythrocyte acanthocytosis (72), leading to significant disability and a reduced life expectancy. Since the discovery of the cause of ChAc, much work has been done to investigate the molecular function of VPS13A. The protein has been localised to endosomal structures in yeast and erythrocytes (14, 28, 64, 70), as well as to the Golgi, and co-fractionates with dense core vesicles in synaptosomes (25, 34). VPS13A is also implicated in a plethora of cellular processes in different setting, including regulation of the actin cytoskeleton (2, 18, 64), protein trafficking (7), membrane morphogenesis (48), autophagy (45) and phagocytosis (59). Cells depleted of VPS13A have decreased levels of PI(4)P and of phosphorylated PI3K (18, 47, 48). Importantly, further evidence for a role for VPS13A in the control of regulated exocytosis was provided recently by Hayashi and colleagues (25), who demonstrated that VPS13A is localized to neurites in dopaminergic PC12 cells. These findings are thus strongly reminiscent of our findings here of colocalisation between VPS13C and insulin in human β cells (Fig. 12). The role for VPS13A in phosphoinositide (PI) metabolism is a function that is conserved between yeast and human orthologues and a possible mechanism by which VPS13A can function in so many different cellular processes (18, 47–49). If VPS13C were to have similar functions in β cells as VPS13A, we would

hypothesise that the former may be involved in protein trafficking, potentially through the regulation of PI metabolism.

Correct regulation of PI metabolism is essential for efficient insulin secretion from β cells (79). Indeed, PI(4)P is the main precursor to form PI(4,5)P₂, which is rapidly turned over to form second messengers required for insulin secretion (68) in a Ca²⁺-dependent manner akin to the release of neurotransmitters from neurons. Interestingly, a distinct role for PI(4)P in signaling from the plasma membrane in the β cell has been suggested (80), since PI(4)P displayed anti-synchronous oscillations compared to PI(4,5)P₂ when MIN6 β cells were stimulated with glucose. A direct role in secretion has already been shown in yeast (24) and it is well known that PI(4)P is involved in membrane trafficking between the Golgi and the plasma membrane and other endosomal compartments (75). Hence VPS13C could function in insulin secretion through regulation of PI metabolism; affecting intracellular insulin trafficking.

Interestingly, new work shows that VPS13C is involved in lipid droplet formation and regulation of galectin-12, and seems to function in adipogenesis (Yang et al, unpublished data). The latter findings indicate that VPS13C may play additional roles in T2D in extra-pancreatic tissues.

Conclusions.

Human islet expression data suggest that variations in the level of expression of *VPS13C* and *C2CD4A* in the β cell may contribute to altered T2D susceptibility in risk allele carriers, at least in females. The relatively mild effects of *Vps13c* ablation on glucose homeostasis are consistent with the hypothesis that changes in the expression of both genes may contribute to overall risk. Future functional studies will be required to determine the role of C2CD4A in the control of insulin secretion, and the possible contribution of indirect mechanisms resulting from changes in the expression of either gene in extrapancreatic tissues.

Acknowledgements

We would also like to thank Dr. Stephen Rothery and the Imperial College FILM facility for training and use of the wide-field microscope. We thank Professor Jorge Ferrer (Imperial College London) for providing plasmid pGL4.23-GW and the *Ins1^{Cre}* mouse line.

Grants

G.A.R. thanks the MRC (UK) for Programme grant MR/J0003042/1, the BBSRC (UK) for a Project grant (BB/J015873/1), the Royal Society for a Wolfson Research Merit Award and the Wellcome Trust for a Senior Investigator Award (WT098424AIA). TJP was a DRWF post-doctoral Fellow (SCA/01/F/12). The work leading to this publication has received support from the Innovative Medicines Initiative Joint Undertaking under grant agreement n° 155005 (IMIDIA), resources of which are composed of a financial contribution from the European Union's Seventh Framework Programme (FP7/2007-2013) and EFPIA companies' in kind contribution (G.A.R., P.M.). Additional support was obtained from a Wellcome Trust core grant (075491/Z/04) and from the Advocacy for Neuroacanthocytosis Patients (to A.P.M. and A.V.-B.).

Author contributions

ZBM coordinated and performed all animal experiments, analysed the data and co-wrote the manuscript with GAR. NF conducted and analysed the luciferase assays and analysed data to calculate β cell mass. MCC designed, performed and analysed the islet perfusion experiments. TJP, MH and NF performed the eQTL analysis. PC generated and used macros to analyse Ca^{2+} dynamics data. GM conducted the staining for VPS13C in human beta cells. AV-B, APM generated rabbit anti-VPS13C antibody and edited the manuscript. LM and PM provided human islets and isolated RNA for eQTL analysis. GAR conceived and coordinated the study and wrote the manuscript with ZBM and TJP.

Disclosures

The authors declare no conflict of interest.

Abbreviations

T2D, Type 2 diabetes; VPS13, vacuolar protein sorting 13; C2CD4A/B, C2 calcium-dependent domain 4A/B; GWAS, genome wide association studies; TCF7L2, transcription factor 7-like 2; LD, linkage disequilibrium; SNP, single nucleotide polymorphism; eQTL, expression quantitative trait *loci*; GSIS, glucose-stimulated insulin secretion; PI(4)P, phosphatidylinositol 4-phosphate; ChAc, Chorea-Acanthocytosis; β *Vps13c*KO, β cell specific VPS13C knockout; RC, regular chow; HFD, high fat diet; Ctrl, control; IPGTT, intraperitoneal glucose tolerance test; OGTT, oral glucose tolerance test; HOMA2, homeostasis model assessment-2; PI, phosphoinositide; PI(4,5)P₂, phosphatidylinositol (4,5)-bisphosphate; AUC, area under the curve; HTRF, homogeneous time-resolved fluorescence.

Figure Legends.

Figure 1: eQTL analysis

The expression of *VPSI3C* (A-C), *C2CD4A* (D-F) and *C2CD4B* (G-I) was quantified relative to *ACTB* in 53 human donor islet samples and compared to the genotype at rs7163757. ΔC_t is plotted against genotype for all samples (A, D and G; $n = 53$) or just samples from male (B, E and H; $n=13$) or female (C, F and I; $n=40$) donors, along with the mean and standard error. Since higher ΔC_t corresponds to lower expression, possession of the risk allele (C) is significantly associated with lower *VPSI3C* expression in samples from female donors ($p=0.041$).

Figure 2: Comparison of promoter/enhancer activities of variants at rs7163757 in the *VPSI3C* locus.

Luciferase reporter assay performed in four cell lines (HEK293, MIN6, 1.1B4 and EndoC- β H1). The risk SNP caused a significant reduction in enhancer activity in HEK293, MIN6 and 1.1B4 (* $p<0.05$, ** $p<0.01$ calculated using ratio paired Student's t-tests). Error bars represent standard error of the mean from either three (HEK293 and MIN6) or four (1.1B4 and EndoC- β H1) independent experiments. $P=0.1$ for the effect of the risk allele in EndoC- β H1 cells.

Figure 3: Generation of *VPSI3C^{fl/fl}::Ins1.Cre^{+/-}* (β *Vps13c*KO) mice.

(A) *LoxP* sites were inserted on either side of exon 1 to enable *Cre*-mediated inactivation of the *Vps13c* gene in pancreatic β cells after breeding to *Ins1.Cre* mice. The resultant colony consisted of *VPSI3C* null mice (KO, β *Vps13c*KO) and control mice (ctrl) at the expected 50:50 ratio.

(B and C) Islets were isolated from 2-3 male (B) and 3 female (C) control and β *Vps13c*KO mice for (i) immunoblotting or (ii) qPCR analysis. Both ΔC_t (relative to *CyclophilinA*) and log2-transformed fold-changes, normalised to control mice, are shown. Error bars represent standard deviation in (ii)

top and 95% confidence intervals in (ii) bottom. *P<0.05; **P<0.01 analysed with 2-way ANOVA with Sidak's multiple corrections.

(D-G) Changes in weight (D and E) and random-fed glycaemia (F and G) over time for Ctrl (black) and $\beta Vps13c$ KO (green dashed, male, or purple dotted, female) mice fed regular chow (RC, circle or square symbols) or HFD (triangle symbols). Inset: area under the curve analysis for female mice on HFD, assessed for significance using an unpaired Student's t-test. $n = 11-15$ mice, as indicated.

Figure 4: Glucose tolerance in male $\beta Vps13c$ KO mice.

(A-H) Intraperitoneal glucose tolerance (1 g/kg body weight) was measured in control (Ctrl; solid black line) and $\beta Vps13c$ KO (KO; dashed green line) male littermates fed either RC (RC, A, C, E, G) or HFD (B, D, F, H). IPGTTs were conducted at 8- (A, B), 12-, (C, D) 16- (E, F) and 20- (G, H) weeks. Inset: area under the curve (AUC). The numbers of animals (n) for each experiment are given in the AUC bars. *P < 0.05; **P<0.01, as assessed with 2-way ANOVA with Fisher's LSD post-hoc test (main graphs) or unpaired Student's t-test (AUC, insets).

Figure 5: Glucose tolerance in female $\beta Vps13c$ KO mice.

(A-H) Intraperitoneal glucose tolerance (1 g/kg body weight) was measured in control (Ctrl; solid black line) and $\beta Vps13c$ KO (KO; dotted purple line) female littermates fed either RC (RC, A, C, E, G) or HFD (B, D, F, H). IPGTTs were conducted at 8- (A, B), 12-, (C, D) 16- (E, F) and 20- (G, H) weeks. Inset: area under the curve (AUC). The numbers of animals (n) for each experiment are given in the AUC bars. *P < 0.05, as assessed with 2-way ANOVA with Fisher's LSD post-hoc test (main graphs) or unpaired Student's t-test (AUC, insets).

Figure 6: Oral glucose tolerance in $\beta Vps13c$ KO and control mice.

(A and B) Oral glucose tolerance (1.5 g/kg body weight) was measured in control (Ctrl; solid black line) and $\beta Vps13c$ KO (KO; dashed green or dotted purple lines) littermates fed RC. OGTTs were conducted at the ages indicated. Inset: area under the curve (AUC). *n* numbers for each experiment are given in the AUC bars. **P* < 0.05; 2-way ANOVA with Fisher's LSD post-hoc test.

Figure 7: Effect of *Vps13C* deletion on GSIS *in vivo*.

(A-D) Plasma insulin concentration was measured following intraperitoneal administration of glucose (3 g/kg body weight) in control (Ctrl; solid black line) and $\beta Vps13c$ KO (KO; dashed green, males, or dotted purple lines, females) littermates. Blood was sampled for insulin measurements when mice were 21- or 19-weeks old (RC or HFD, respectively). Inset (top): respective glycaemia measurements. Inset (bottom): area under the curve calculated from the main graph, measuring total released plasma insulin. *n* = 6-9 mice per genotype, as detailed in the key.

(E-H) HOMA2-%B (E and G) and %S (F and H) analysis using fasting glycaemia values and corresponding plasma insulin concentrations. ***P* < 0.01; unpaired Student's *t*-test with Welch's correction (E-H).

Figure 8: Effect of *Vps13c* deletion on GSIS *in vitro*.

(A-D) Insulin secretion from isolated islets from $\beta Vps13c$ KO and control mice over 20 weeks old maintained on either RC (A and C) or HFD (B and D) was assessed by incubating 10 size-matched islets in Krebs's-Ringer solution containing 3 mM glucose (3 Glu), 16.7 mM glucose (16.7 Glu) or 20 mM KCl for 30 min. and measuring the amount of insulin secreted (see Materials and Methods). Islets were lysed to measure total insulin; results are presented as % of total insulin. (E) Insulin secretion from islets continuously perfused with Krebs's-Ringer solution containing 3 mM glucose and then stimulated with 16.7 mM glucose. *n* = 3-5 mice per genotype, as indicated. **P* < 0.05; ***P* < 0.01; ****P* < 0.001; *****P* < 0.0001; 2-way ANOVA with Sidak or Tukey's post-hoc test where appropriate.

632

633 **Figure 9: β -cell mass in $\beta Vps13c$ KO mice.**

634 (A and C) Representative images from pancreatic slices from female (A) and male (B) control and
635 $\beta Vps13c$ KO mice (20-23 weeks of age) fed a RC diet. Slices were stained with antibodies against
636 insulin (green) and glucagon (red). Nuclei were stained with DAPI; scale bar represents 50 μ m.

637 (B and D) Percentage of β (i) and α (ii) cell surface area, normalised to whole pancreas surface area.
638 (iii) β/α cell ratio.

639 Data are from $n = 3$ control and 3 KO (females); 3 control and 5 KO (males). No significant
640 differences between genotypes were detected.

641

642 **Figure 10: Effect of $Vps13c$ deletion on calcium signalling *in vitro* in male mouse islets.**

643 Isolated islets from male mice (20-23 weeks of age), maintained on either RC (A) or HFD (B) were
644 loaded with Fluo-2 and incubated in Kreb's-Ringer solution containing 3 mM glucose (3mM Glu) for
645 45 min. Dye-loaded islets (3-7 per field of view) were imaged on a spinning disk confocal microscope
646 for 2 min in 3 mM glucose, as described under Materials and Methods. A perfusion system was used
647 to allow subsequent imaging of the islets in 16.7 mM Glu for 18 min, followed by 20 mM KCl for 5
648 min. Individual traces from each islet were then averaged to give one trace per islet, which was then
649 pooled with the other islets. (i) Mean free Ca^{2+} (normalised to initial fluorescence; F/F_0); (ii) inset
650 from (i), mean free Ca^{2+} measured between 300 and 500 s, showing the effect of stimulation with 16.7
651 mM glucose. (iii) Area under the curve (AUC) analysis for high glucose stimulation; (iv) AUC
652 analysis for KCl stimulation. (v) Time to maximum peak value from stimulation with glucose; (vi)
653 maximum peak value (F/F_0) from stimulation with glucose; (vii) time to maximum peak value from
654 stimulation with KCl; (viii) maximum peak value (F/F_0) from stimulation with KCl. $n = 3$ -5 mice per
655 genotype; number of islets (n) used: $n =$ male RC 31-38 islets from 3 mice; male HFD mice $n = 41$ -46
656 islets from 4 mice. * $P < 0.05$; ** $P < 0.01$; *** $P < 0.001$; unpaired Student's t-test.

657

658 **Figure 11: Effect of *Vps13c* deletion on calcium signaling *in vitro* in female mouse islets.**

659 Isolated islets from female mice (20-23 weeks of age) maintained on either RC (A) or HFD (B) were
660 loaded with Fluo-2 and analysed as for male islets (Fig. 10). (i) Mean free calcium (F/F0); (ii) inset
661 from (i), mean free calcium measured between 300 and 500 s, showing stimulation with 16.7 mM
662 glucose. (iii) Area under the curve analysis for high glucose stimulation; (iv) area under the curve
663 analysis for KCl stimulation. (v) Time to maximum peak value from stimulation with glucose; (vi)
664 maximum peak value (F/F0) from stimulation with glucose; (vii) time to maximum peak value from
665 stimulation with KCl; (viii) maximum peak value (F/F0) from stimulation with KCl. *n* = 3-5 mice per
666 genotype; number of islets (*n*) used: female RC *n* = 47-48 islets from 4 mice; female HFD *n* = 46-59
667 islets from 4 or 5 mice (β *Vps13c*KO vs. ctrl, respectively). **P*<0.5; ***P*<0.01; ****P*<0.001; unpaired
668 Student's t-test.

669

670 **Figure 12: Subcellular localisation of VPS13C in human β cells.** Immunocytochemical analysis for
671 insulin (green) and VPS13C (red) was performed using confocal microscopy in single β cells as
672 described under Materials and Methods. Scale bar represents 10 μ m.

673

674

675

676

677

678

679

680 References

- 681 1. **Abramoff MD, Magelhaes PJ, Ram SJ.** Image Processing with ImageJ. *Biophotonics Int* 11:
682 36–42, 2004.
- 683 2. **Alesutan I, Seifert J, Pakladok T, Rheinlaender J, Lebedeva A, Towhid ST, Stournaras C,**
684 **Voelkl J, Schäffer TE, Lang F.** Chorea Sensitivity of Actin Polymerization, Cell Shape and
685 Mechanical Stiffness of Vascular Endothelial Cells. *Cell Physiol Biochem* 32: 728–742, 2013.
- 686 3. **Almaça J, Molina J, Drigo RA e, Abdulreda MH, Jeon WB, Berggren P-O, Caicedo A,**
687 **Nam HG.** Young capillary vessels rejuvenate aged pancreatic islets. *Proc Natl Acad Sci* 111:
688 17612–17617, 2014.
- 689 4. **Baroukh N, Ravier MA, Loder MK, Hill EV, Bounacer A, Scharfmann R, Rutter GA,**
690 **Obberghen EV.** MicroRNA-124a Regulates Foxa2 Expression and Intracellular Signaling in
691 Pancreatic β -Cell Lines. *J Biol Chem* 282: 19575–19588, 2007.
- 692 5. **Benner C, van der Meulen T, Cacères E, Tigyi K, Donaldson CJ, Huising MO.** The
693 transcriptional landscape of mouse beta cells compared to human beta cells reveals notable
694 species differences in long non-coding RNA and protein-coding gene expression. *BMC*
695 *Genomics* 15: 620, 2014.
- 696 6. **Boesgaard TW, Grarup N, Jørgensen T, Borch-Johnsen K, Hansen T, Pedersen O, (magic)**
697 **M-A of G and I-RTC.** Variants at DGKB/TMEM195, ADRA2A, GLIS3 and C2CD4B loci are
698 associated with reduced glucose-stimulated beta cell function in middle-aged Danish people.
699 *Diabetologia* 53: 1647–1655, 2010.
- 700 7. **Brickner JH, Fuller RS.** SOI1 Encodes a Novel, Conserved Protein That Promotes TGN–
701 Endosomal Cycling of Kex2p and Other Membrane Proteins by Modulating the Function of
702 Two TGN Localization Signals. *J Cell Biol* 139: 23–36, 1997.
- 703 8. **Brouwers B, de Faudeur G, Osipovich AB, Goyvaerts L, Lemaire K, Boesmans L,**
704 **Cauwelier EJG, Granvik M, Pruniau VPEG, Van Lommel L, Van Schoors J, Stancill JS,**
705 **Smolders I, Goffin V, Binart N, in't Veld P, Declercq J, Magnuson MA, Creemers JWM,**
706 **Schuit F, Schraenen A.** Impaired Islet Function in Commonly Used Transgenic Mouse Lines
707 due to Human Growth Hormone Minigene Expression. *Cell Metab* 20: 979–990, 2014.
- 708 9. **van de Bunt M, Manning Fox JE, Dai X, Barrett A, Grey C, Li L, Bennett AJ, Johnson**
709 **PR, Rajotte RV, Gaulton KJ, Dermitzakis ET, MacDonald PE, McCarthy MI, Gloyn AL.**
710 Transcript Expression Data from Human Islets Links Regulatory Signals from Genome-Wide
711 Association Studies for Type 2 Diabetes and Glycemic Traits to Their Downstream Effectors.
712 *PLoS Genet* 11: e1005694, 2015.
- 713 10. **Cane MC, Parrington J, Rorsman P, Galione A, Rutter GA.** The two pore channel TPC2 is
714 dispensable in pancreatic β -cells for normal Ca^{2+} dynamics and insulin secretion. *Cell Calcium*
715 (2015). doi: 10.1016/j.ceca.2015.12.004.
- 716 11. **Creager MA, Lüscher TF, Of P with the A, Cosentino F, Beckman JA.** Diabetes and
717 Vascular Disease Pathophysiology, Clinical Consequences, and Medical Therapy: Part I.
718 *Circulation* 108: 1527–1532, 2003.
- 719 12. **Cui B, Zhu X, Xu M, Guo T, Zhu D, Chen G, Li X, Xu L, Bi Y, Chen Y, Xu Y, Li X, Wang**
720 **W, Wang H, Huang W, Ning G.** A Genome-Wide Association Study Confirms Previously
721 Reported Loci for Type 2 Diabetes in Han Chinese. *PLoS ONE* 6: e22353, 2011.

13. Diabetes Genetics Initiative of Broad Institute of Harvard and MIT, Lund University and Novartis Institutes of Biomedical Research, Saxena R, Voight BF, Lyssenko V, Burt NP, Bakker PIW de, Chen H, Roix JJ, Kathiresan S, Hirschhorn JN, Daly MJ, Hughes TE, Groop L, Altshuler D, Almgren P, Florez JC, Meyer J, Ardlie K, Boström KB, Isomaa B, Lettre G, Lindblad U, Lyon HN, Melander O, Newton-Cheh C, Nilsson P, Orho-Melander M, Råstam L, Speliotes EK, Taskinen M-R, Tuomi T, Guiducci C, Berglund A, Carlson J, Gianniny L, Hackett R, Hall L, Holmkvist J, Laurila E, Sjögren M, Sterner M, Surti A, Svensson M, Svensson M, Tewhey R, Blumenstiel B, Parkin M, DeFelice M, Barry R, Brodeur W, Camarata J, Chia N, Fava M, Gibbons J, Handsaker B, Healy C, Nguyen K, Gates C, Sougnez C, Gage D, Nizzari M, Gabriel SB, Chirn G-W, Ma Q, Parikh H, Richardson D, Rieke D, Purcell S. Genome-Wide Association Analysis Identifies Loci for Type 2 Diabetes and Triglyceride Levels. *Science* 316: 1331–1336, 2007.
14. Dobson-Stone C, Velayos-Baeza A, Filippone LA, Westbury S, Storch A, Erdmann T, Wroe SJ, Leenders KL, Lang AE, Dotti MT, Federico A, Mohiddin SA, Fananapazir L, Daniels G, Danek A, Monaco AP. Chorein detection for the diagnosis of chorea-acanthocytosis. *Ann Neurol* 56: 299–302, 2004.
15. Dupuis J, Langenberg C, Prokopenko I, Saxena R, Soranzo N, Jackson AU, Wheeler E, Glazer NL, Bouatia-Naji N, Gloyn AL, Lindgren CM, Mägi R, Morris AP, Randall J, Johnson T, Elliott P, Rybin D, Thorleifsson G, Steinthorsdottir V, Henneman P, Grallert H, Dehghan A, Hottenga JJ, Franklin CS, Navarro P, Song K, Goel A, Perry JRB, Egan JM, Lajunen T, Grarup N, Sparso T, Doney A, Voight BF, Stringham HM, Li M, Kanoni S, Shrader P, Cavalcanti-Proença C, Kumari M, Qi L, Timpson NJ, Gieger C, Zabena C, Rocheleau G, Ingelsson E, An P, O’Connell J, Luan J ’an, Elliott A, McCarroll SA, Payne F, Roccascaccia RM, Pattou F, Sethupathy P, Ardlie K, Ariyurek Y, Balkau B, Barter P, Beilby JP, Ben-Shlomo Y, Benediktsson R, Bennett AJ, Bergmann S, Bochud M, Boerwinkle E, Bonnefond A, Bonnycastle LL, Borch-Johnsen K, Böttcher Y, Brunner E, Bumpstead SJ, Charpentier G, Chen Y-DI, Chines P, Clarke R, Coin LJM, Cooper MN, Cornelis M, Crawford G, Crisponi L, Day INM, Geus EJC de, Delplanque J, Dina C, Erdos MR, Fedson AC, Fischer-Rosinsky A, Forouhi NG, Fox CS, Frants R, Franzosi MG, Galan P, Goodarzi MO, Graessler J, Groves CJ, Grundy S, Gwilliam R, Gyllenstein U, Hadjadj S, Hallmans G, Hammond N, Han X, Hartikainen A-L, Hassanali N, Hayward C, Heath SC, Herberg S, Herder C, Hicks AA, Hillman DR, Hingorani AD, Hofman A, Hui J, Hung J, Isomaa B, Johnson PRV, Jørgensen T, Jula A, Kaakinen M, Kaprio J, Kesaniemi YA, Kivimäki M, Knight B, Kosken S, Kovacs P, Kyvik KO, Lathrop GM, Lawlor DA, Le Bacquer O, Lecoeur C, Li Y, Lyssenko V, Mahley R, Mangino M, Manning AK, Martínez-Larrad MT, McAteer JB, McCulloch LJ, McPherson R, Meisinger C, Melzer D, Meyre D, Mitchell BD, Morken MA, Mukherjee S, Naitza S, Narisu N, Neville MJ, Oostra BA, Orrù M, Pakyz R, Palmer CNA, Paolisso G, Pattaro C, Pearson D, Peden JF, Pedersen NL, Perola M, Pfeiffer AFH, Pichler I, Polasek O, Posthuma D, Potter SC, Pouta A, Province MA, Psaty BM, Rathmann W, Rayner NW, Rice K, Ripatti S, Rivadeneira F, Roden M, Rolandsson O, Sandbaek A, Sandhu M, Sanna S, Sayer AA, Scheet P, Scott LJ, Sedorf U, Sharp SJ, Shields B, Sigurðsson G, Sijbrands EJG, Silveira A, Simpson L, Singleton A, Smith NL, Sovio U, Swift A, Syddall H, Syvänen A-C, Tanaka T, Thorand B, Tichet J, Tönjes A, Tuomi T, Uitterlinden AG, van Dijk KW, van Hoek M, Varma D, Visvikis-Siest S, Vitart V, Vogelzangs N, Waeber G, Wagner PJ, Walley A, Walters GB, Ward KL, Watkins H, Weedon MN, Wild SH, Willemssen G, Witteman JCM, Yarnell JWG, Zeggini E, Zelenika D, Zethelius B, Zhai G, Zhao JH, Zillikens MC, Consortium D, Consortium G, Consortium GBp, Borecki IB, Loos RJJ, Meneton P, Magnusson PKE, Nathan DM, Williams GH, Hattersley AT, Silander K, Salomaa V, Smith GD, Bornstein SR, Schwarz P, Spranger J, Karpe F, Shuldiner AR, Cooper C, Dedoussis GV, Serrano-Ríos M, Morris AD, Lind L, Palmer LJ, Hu FB, Franks PW, Ebrahim S, Marmot M, Kao WHL, Pankow JS, Sampson MJ, Kuusisto J, Laakso M, Hansen T, Pedersen O, Pramstaller PP, Wichmann HE, Illig T, Rudan I, Wright AF,

- 775 **Stumvoll M, Campbell H, Wilson JF, Consortium AH on behalf of P, Investigators the M.**
 776 **New genetic loci implicated in fasting glucose homeostasis and their impact on type 2 diabetes**
 777 **risk. *Nat Genet* 42: 105–116, 2010.**
- 778 16. **Elayat AA, el-Naggar MM, Tahir M.** An immunocytochemical and morphometric study of the
 779 **rat pancreatic islets. *J Anat* 186: 629–637, 1995.**
- 780 17. **Fadista J, Vikman P, Laakso EO, Mollet IG, Esguerra JL, Taneera J, Storm P, Osmark P,**
 781 **Ladenvall C, Prasad RB, Hansson KB, Finotello F, Uvebrant K, Ofori JK, Camillo BD,**
 782 **Krus U, Cilio CM, Hansson O, Eliasson L, Rosengren AH, Renström E, Wollheim CB,**
 783 **Groop L.** Global genomic and transcriptomic analysis of human pancreatic islets reveals novel
 784 **genes influencing glucose metabolism. *Proc Natl Acad Sci* 111: 13924–13929, 2014.**
- 785 18. **Föller M, Hermann A, Gu S, Alesutan I, Qadri SM, Borst O, Schmidt E-M, Schiele F,**
 786 **Hagen JM vom, Saft C, Schöls L, Lerche H, Stournaras C, Storch A, Lang F.** Chorein-
 787 **sensitive polymerization of cortical actin and suicidal cell death in chorea-acanthocytosis.**
 788 ***FASEB J* 26: 1526–1534, 2012.**
- 789 19. **Fowler MJ.** Microvascular and Macrovascular Complications of Diabetes. *Clin Diabetes* 26:
 790 **77–82, 2008.**
- 791 20. **Gaulton KJ, Ferreira T, Lee Y, Raimondo A, Mägi R, Reschen ME, Mahajan A, Locke A,**
 792 **William Rayner N, Robertson N, Scott RA, Prokopenko I, Scott LJ, Green T, Sparso T,**
 793 **Thuillier D, Yengo L, Grallert H, Wahl S, Frånberg M, Strawbridge RJ, Kestler H,**
 794 **Chheda H, Eisele L, Gustafsson S, Steinthorsdottir V, Thorleifsson G, Qi L, Karssen LC,**
 795 **van Leeuwen EM, Willems SM, Li M, Chen H, Fuchsberger C, Kwan P, Ma C, Linderman**
 796 **M, Lu Y, Thomsen SK, Rundle JK, Beer NL, van de Bunt M, Chalisey A, Kang HM,**
 797 **Voight BF, Abecasis GR, Almgren P, Baldassarre D, Balkau B, Benediktsson R, Blüher M,**
 798 **Boeing H, Bonnycastle LL, Bottinger EP, Burt NP, Carey J, Charpentier G, Chines PS,**
 799 **Cornelis MC, Couper DJ, Crenshaw AT, van Dam RM, Doney ASF, Dorkhan M, Edkins**
 800 **S, Eriksson JG, Esko T, Eury E, Fadista J, Flannick J, Fontanillas P, Fox C, Franks PW,**
 801 **Gertow K, Gieger C, Gigante B, Gottesman O, Grant GB, Grarup N, Groves CJ, Hassinen**
 802 **M, Have CT, Herder C, Holmen OL, Hreidarsson AB, Humphries SE, Hunter DJ, Jackson**
 803 **AU, Jonsson A, Jørgensen ME, Jørgensen T, Kao W-HL, Kerrison ND, Kinnunen L,**
 804 **Klopp N, Kong A, Kovacs P, Kraft P, Kravic J, Langford C, Leander K, Liang L, Lichtner**
 805 **P, Lindgren CM, Lindholm E, Linneberg A, Liu C-T, Lobbens S, Luan J 'an, Lyssenko V,**
 806 **Männistö S, McLeod O, Meyer J, Mihailov E, Mirza G, Mühleisen TW, Müller-Nurasyid**
 807 **M, Navarro C, Nöthen MM, Oskolkov NN, Owen KR, Palli D, Pechlivanis S, Peltonen L,**
 808 **Perry JRB, Platou CGP, Roden M, Ruderfer D, Rybin D, van der Schouw YT, Sennblad**
 809 **B, Sigurðsson G, Stančáková A, Steinbach G, Storm P, Strauch K, Stringham HM, Sun Q,**
 810 **Thorand B, Tikkanen E, Tonjes A, Trakalo J, Tremoli E, Tuomi T, Wennauer R,**
 811 **Wiltshire S, Wood AR, Zeggini E, Dunham I, Birney E, Pasquali L, Ferrer J, Loos RJF,**
 812 **Dupuis J, Florez JC, Boerwinkle E, Pankow JS, van Duijn C, Sijbrands E, Meigs JB, Hu**
 813 **FB, Thorsteinsdottir U, Stefansson K, Lakka TA, Rauramaa R, Stumvoll M, Pedersen NL,**
 814 **Lind L, Keinanen-Kiukaanniemi SM, Korpi-Hyövälti E, Saaristo TE, Saltevo J, Kuusisto**
 815 **J, Laakso M, Metspalu A, Erbel R, Jöcke K-H, Moebus S, Ripatti S, Salomaa V, Ingelsson**
 816 **E, Boehm BO, Bergman RN, Collins FS, Mohlke KL, Koistinen H, Tuomilehto J, Hveem**
 817 **K, Njølstad I, Deloukas P, Donnelly PJ, Frayling TM, Hattersley AT, de Faire U, Hamsten**
 818 **A, Illig T, Peters A, Cauchi S, Sladek R, Froguel P, Hansen T, Pedersen O, Morris AD,**
 819 **Palmer CNA, Kathiresan S, Melander O, Nilsson PM, Groop LC, Barroso I, Langenberg**
 820 **C, Wareham NJ, O'Callaghan CA, Gloyn AL, Altshuler D, Boehnke M, Teslovich TM,**
 821 **McCarthy MI, Morris AP, the DIAbetes Genetics Replication And Meta-analysis**
 822 **(DIAGRAM) Consortium.** Genetic fine mapping and genomic annotation defines causal
 823 **mechanisms at type 2 diabetes susceptibility loci. *Nat Genet* 47: 1415–1425, 2015.**

- 824 21. Grant SFA, Thorleifsson G, Reynisdottir I, Benediktsson R, Manolescu A, Sainz J,
825 Helgason A, Stefansson H, Emilsson V, Helgadottir A, Styrkarsdottir U, Magnusson KP,
826 Walters GB, Palsdottir E, Jonsdottir T, Gudmundsdottir T, Gylfason A, Saemundsdottir
827 J, Wilensky RL, Reilly MP, Rader DJ, Bagger Y, Christiansen C, Gudnason V, Sigurdsson
828 G, Thorsteinsdottir U, Gulcher JR, Kong A, Stefansson K. Variant of transcription factor 7-
829 like 2 (TCF7L2) gene confers risk of type 2 diabetes. *Nat Genet* 38: 320–323, 2006.
- 830 22. Grarup N, Overvad M, Sparso T, Witte DR, Pisinger C, Jørgensen T, Yamauchi T, Hara
831 K, Maeda S, Kadowaki T, Hansen T, Pedersen O. The diabetogenic
832 VPS13C/C2CD4A/C2CD4B rs7172432 variant impairs glucose-stimulated insulin response in
833 5,722 non-diabetic Danish individuals. *Diabetologia* 54: 789–794, 2011.
- 834 23. Groves CJ, Zeggini E, Minton J, Frayling TM, Weedon MN, Rayner NW, Hitman GA,
835 Walker M, Wiltshire S, Hattersley AT, McCarthy MI. Association Analysis of 6,736 U.K.
836 Subjects Provides Replication and Confirms TCF7L2 as a Type 2 Diabetes Susceptibility Gene
837 With a Substantial Effect on Individual Risk. *Diabetes* 55: 2640–2644, 2006.
- 838 24. Hama H, Schnieders EA, Thorner J, Takemoto JY, DeWald DB. Direct Involvement of
839 Phosphatidylinositol 4-Phosphate in Secretion in the Yeast *Saccharomyces cerevisiae*. *J Biol*
840 *Chem* 274: 34294–34300, 1999.
- 841 25. Hayashi T, Kishida M, Nishizawa Y, Iijima M, Koriyama C, Nakamura M, Sano A,
842 Kishida S. Subcellular localization and putative role of VPS13A/chorein in dopaminergic
843 neuronal cells. *Biochem Biophys Res Commun* 419: 511–516, 2012.
- 844 26. Helman A, Klochendler A, Azazmeh N, Gabai Y, Horwitz E, Anzi S, Swisa A, Condiotti R,
845 Granit RZ, Nevo Y, Fixler Y, Shreibman D, Zamir A, Tornovsky-Babeay S, Dai C, Glaser
846 B, Powers AC, Shapiro AMJ, Magnuson MA, Dor Y, Ben-Porath I. p16Ink4a-induced
847 senescence of pancreatic beta cells enhances insulin secretion. *Nat Med* 22: 412–420, 2016.
- 848 27. Hodson DJ, Mitchell RK, Bellomo EA, Sun G, Vinet L, Meda P, Li D, Li W-H, Bugliani M,
849 Marchetti P, Bosco D, Piemonti L, Johnson P, Hughes SJ, Rutter GA. Lipotoxicity disrupts
850 incretin-regulated human β cell connectivity. *J Clin Invest* 123: 4182–4194, 2013.
- 851 28. Huh W-K, Falvo JV, Gerke LC, Carroll AS, Howson RW, Weissman JS, O'Shea EK.
852 Global analysis of protein localization in budding yeast. *Nature* 425: 686–691, 2003.
- 853 29. Ingelsson E, Langenberg C, Hivert M-F, Prokopenko I, Lyssenko V, Dupuis J, Mägi R,
854 Sharp S, Jackson AU, Assimes TL, Shrader P, Knowles JW, Zethelius B, Abbasi FA,
855 Bergman RN, Bergmann A, Berne C, Boehnke M, Bonnycastle LL, Bornstein SR,
856 Buchanan TA, Bumpstead SJ, Böttcher Y, Chines P, Collins FS, Cooper CC, Dennison
857 EM, Erdos MR, Ferrannini E, Fox CS, Graessler J, Hao K, Isomaa B, Jameson KA,
858 Kovacs P, Kuusisto J, Laakso M, Ladenvall C, Mohlke KL, Morken MA, Narisu N,
859 Nathan DM, Pascoe L, Payne F, Petrie JR, Sayer AA, Schwarz PEH, Scott LJ, Stringham
860 HM, Stumvoll M, Swift AJ, Syvänen A-C, Tuomi T, Tuomilehto J, Tönjes A, Valle TT,
861 Williams GH, Lind L, Barroso I, Quertermous T, Walker M, Wareham NJ, Meigs JB,
862 McCarthy MI, Groop L, Watanabe RM, Florez JC, Investigators on behalf of the M.
863 Detailed Physiologic Characterization Reveals Diverse Mechanisms for Novel Genetic Loci
864 Regulating Glucose and Insulin Metabolism in Humans. *Diabetes* 59: 1266–1275, 2010.
- 865 30. International Diabetes Federation. IDF Diabetes Atlas [Online]. 6th ed.
866 <http://www.idf.org/diabetesatlas>.
- 867 31. Kahn SE, Hull RL, Utzschneider KM. Mechanisms linking obesity to insulin resistance and
868 type 2 diabetes. *Nature* 444: 840–846, 2006.

- 869 32. Kolehmainen J, Black GCM, Saarinen A, Chandler K, Clayton-Smith J, Träskelin A-L,
870 Perveen R, Kivitie-Kallio S, Norio R, Warburg M, Fryns J-P, Chapelle A de la, Lehesjoki
871 A-E. Cohen Syndrome Is Caused by Mutations in a Novel Gene, COH1, Encoding a
872 Transmembrane Protein with a Presumed Role in Vesicle-Mediated Sorting and Intracellular
873 Protein Transport. *Am J Hum Genet* 72: 1359–1369, 2003.
- 874 33. Kone M, Pullen TJ, Sun G, Ibberson M, Martinez-Sanchez A, Sayers S, Nguyen-Tu M-S,
875 Kantor C, Swisa A, Dor Y, Gorman T, Ferrer J, Thorens B, Reimann F, Gribble F,
876 McGinty JA, Chen L, French PM, Birzele F, Hildebrandt T, Uphues I, Rutter GA. LKB1
877 and AMPK differentially regulate pancreatic β -cell identity. *FASEB J* 28: 4972–4985, 2014.
- 878 34. Kurano Y, Nakamura M, Ichiba M, Matsuda M, Mizuno E, Kato M, Agemura A, Izumo S,
879 Sano A. In vivo distribution and localization of chorein. *Biochem Biophys Res Commun* 353:
880 431–435, 2007.
- 881 35. Lesage S, Drouet V, Majounie E, Deramecourt V, Jacoupy M, Nicolas A, Cormier-
882 Dequaire F, Hassoun SM, Pujol C, Ciura S, Erpapazoglou Z, Usenko T, Maurage C-A,
883 Sahbatou M, Liebau S, Ding J, Bilgic B, Emre M, Erginel-Unaltuna N, Guven G, Tison F,
884 Tranchant C, Vidailhet M, Corvol J-C, Krack P, Leutenegger A-L, Nalls MA, Hernandez
885 DG, Heutink P, Gibbs JR, Hardy J, Wood NW, Gasser T, Durr A, Deleuze J-F, Tazir M,
886 Destée A, Lohmann E, Kabashi E, Singleton A, Corti O, Brice A, Lesage S, Tison F,
887 Vidailhet M, Corvol J-C, Agid Y, Anheim M, Bonnet A-M, Borg M, Broussolle E, Damier
888 P, Destée A, Dürr A, Durif F, Krack P, Klebe S, Lohmann E, Martinez M, Pollak P, Rascol
889 O, Tranchant C, Vérin M, Viallet F, Brice A, Lesage S, Majounie E, Tison F, Vidailhet M,
890 Corvol JC, Nalls MA, Hernandez DG, Gibbs JR, Dürr A, Arepalli S, Barker RA, Ben-
891 Shlomo Y, Berg D, Bettella F, Bhatia K, de Bie RMA, Biffi A, Bloem BR, Bochdanovits Z,
892 Bonin M, Lesage S, Tison F, Vidailhet M, Corvol J-C, Agid Y, Anheim M, Bonnet A-M,
893 Borg M, Broussolle E, Damier P, Destée A, Dürr A, Durif F, Krack P, Klebe S, Lohmann
894 E, Martinez M, Pollak P, Rascol O, Tranchant C, Vérin M, Bras JM, Brockmann K,
895 Brooks J, Burn DJ, Charlesworth G, Chen H, Chinnery PF, Chong S, Clarke CE, Cookson
896 MR, Counsell C, Damier P, Dartigues J-F, Deloukas P, Deuschl G, Dexter DT, van Dijk
897 KD, Dillman A, Dong J, Durif F, Edkins S, Escott-Price V, Evans JR, Foltyniec T, Gao J,
898 Gardner M, Goate A, Gray E, Guerreiro R, Harris C, van Hilten JJ, Hofman A,
899 Hollenbeck A, Holmans P, Holton J, Hu M, Huang X, Huber H, Hudson G, Hunt SE,
900 Huttenlocher J, Illig T, Jónsson PV, Kilarski LL, Jansen IE, Lambert J-C, Langford C,
901 Lees A, Lichtner P, Limousin P, Lopez G, Lorenz D, Lubbe S, Lungu C, Martinez M,
902 Mätzler W, McNeill A, Moorby C, Moore M, Morrison KE, Mudanohwo E, O’Sullivan SS,
903 Owen MJ, Pearson J, Perlmutter JS, Pétursson H, Plagnol V, Pollak P, Post B, Potter S,
904 Ravina B, Revesz T, Riess O, Rivadeneira F, Rizzu P, Ryten M, Saad M, Simón-Sánchez J,
905 Sawcer S, Schapira A, Scheffer H, Schulte C, Sharma M, Shaw K, Sheerin U-M, Shoulson
906 I, Shulman J, Sidransky E, Spencer CCA, Stefánsson H, Stefánsson K, Stockton JD,
907 Strange A, Talbot K, Tanner CM, Tashakkori-Ghanbaria A, Trabzuni D, Traynor BJ,
908 Uitterlinden AG, Velseboer D, Walker R, van de Warrenburg B, Wickremaratchi M,
909 Williams-Gray CH, Winder-Rhodes S, Wurster I, Williams N, Morris HR, Heutink P,
910 Hardy J, Wood NW, Gasser T, Singleton AB, Brice A. Loss of VPS13C Function in
911 Autosomal-Recessive Parkinsonism Causes Mitochondrial Dysfunction and Increases
912 PINK1/Parkin-Dependent Mitophagy. *Am J Hum Genet* 98: 500–513, 2016.
- 913 36. Levy JC, Matthews DR, Hermans MP. Correct Homeostasis Model Assessment (HOMA)
914 Evaluation Uses the Computer Program. *Diabetes Care* 21: 2191, 1998.
- 915 37. Limoge F, Faivre L, Gautier T, Petit J-M, Gautier E, Masson D, Jegu G, Chehadeh-
916 Djebbar SE, Marle N, Carmignac V, Deckert V, Brindisi M-C, Edery P, Ghoumid J, Blair
917 E, Lagrost L, Thauvin-Robinet C, Duplomb L. Insulin response dysregulation explains

- 918 abnormal fat storage and increased risk of diabetes mellitus type 2 in Cohen Syndrome. *Hum*
919 *Mol Genet* 24: 6603–6613, 2015.
- 920 38. **Ma D, Shield JPH, Dean W, Leclerc I, Knauf C, Burcelin R, Rutter GA, Kelsey G.**
921 Impaired glucose homeostasis in transgenic mice expressing the human transient neonatal
922 diabetes mellitus locus, TNDM. *J Clin Invest* 114: 339–348, 2004.
- 923 39. **Marselli L, Thorne J, Dahiya S, Sgroi DC, Sharma A, Bonner-Weir S, Marchetti P, Weir**
924 **GC.** Gene Expression Profiles of Beta-Cell Enriched Tissue Obtained by Laser Capture
925 Microdissection from Subjects with Type 2 Diabetes. *PLOS ONE* 5: e11499, 2010.
- 926 40. **Marullo L, Moustafa JSE-S, Prokopenko I.** Insights into the Genetic Susceptibility to Type 2
927 Diabetes from Genome-Wide Association Studies of Glycaemic Traits. *Curr Diab Rep* 14: 1–
928 17, 2014.
- 929 41. **McCluskey JT, Hamid M, Guo-Parke H, McClenaghan NH, Gomis R, Flatt PR.**
930 Development and Functional Characterization of Insulin-releasing Human Pancreatic Beta Cell
931 Lines Produced by Electrofusion. *J Biol Chem* 286: 21982–21992, 2011.
- 932 42. **Meur G, Simon A, Harun N, Virally M, Dechaume A, Bonnefond A, Fetita S, Tarasov AI,**
933 **Guillausseau P-J, Boesgaard TW, Pedersen O, Hansen T, Polak M, Gautier J-F, Froguel**
934 **P, Rutter GA, Vaxillaire M.** Insulin Gene Mutations Resulting in Early-Onset Diabetes:
935 Marked Differences in Clinical Presentation, Metabolic Status, and Pathogenic Effect Through
936 Endoplasmic Reticulum Retention. *Diabetes* 59: 653–661, 2010.
- 937 43. **Mitchell RK, Mondragon A, Chen L, McGinty JA, French PM, Ferrer J, Thorens B,**
938 **Hodson DJ, Rutter GA, Xavier GDS.** Selective disruption of Tcf7l2 in the pancreatic β cell
939 impairs secretory function and lowers β cell mass. *Hum Mol Genet* 24: 1390–1399, 2015.
- 940 44. **Miyazaki J-I, Araki K, Yamato E, Ikegami H, Asano T, Shibasaki Y, Oka Y, Yamamura**
941 **K-I.** Establishment of a Pancreatic β Cell Line That Retains Glucose-Inducible Insulin
942 Secretion: Special Reference to Expression of Glucose Transporter Isoforms. *Endocrinology*
943 127: 126–132, 1990.
- 944 45. **Muñoz-Bracerás S, Calvo R, Escalante R.** TipC and the chorea-acanthocytosis protein
945 VPS13A regulate autophagy in Dictyostelium and human HeLa cells. *Autophagy* 11: 918–927,
946 2015.
- 947 46. **Nadal A, Alonso-Magdalena P, Soriano S, Ripoll C, Fuentes E, Quesada I, Ropero AB.**
948 Role of estrogen receptors alpha, beta and GPER1/GPR30 in pancreatic beta-cells. *Front Biosci*
949 *Landmark Ed* 16: 251–260, 2011.
- 950 47. **Park J-S, Halegoua S, Kishida S, Neiman AM.** A Conserved Function in Phosphatidylinositol
951 Metabolism for Mammalian Vps13 Family Proteins. *PLoS ONE* 10: e0124836, 2015.
- 952 48. **Park J-S, Neiman AM.** VPS13 regulates membrane morphogenesis during sporulation in
953 *Saccharomyces cerevisiae*. *J Cell Sci* 125: 3004–3011, 2012.
- 954 49. **Park J-S, Okumura Y, Tachikawa H, Neiman AM.** SPO71 Encodes a Developmental Stage-
955 Specific Partner for Vps13 in *Saccharomyces cerevisiae*. *Eukaryot Cell* 12: 1530–1537, 2013.
- 956 50. **Parker SCJ, Stitzel ML, Taylor DL, Orozco JM, Erdos MR, Akiyama JA, van Bueren KL,**
957 **Chines PS, Narisu N, NISC Comparative Sequencing Program, Black BL, Visel A,**
958 **Pennacchio LA, Collins FS, National Institutes of Health Intramural Sequencing Center**
959 **Comparative Sequencing Program Authors, NISC Comparative Sequencing Program**

- 960 **Authors.** Chromatin stretch enhancer states drive cell-specific gene regulation and harbor
961 human disease risk variants. *Proc Natl Acad Sci U S A* 110: 17921–17926, 2013.
- 962 51. **Prudente S, Morini E, Marselli L, Baratta R, Copetti M, Mendonca C, Andreozzi F,**
963 **Chandalia M, Pellegrini F, Bailetti D, Alberico F, Shah H, Abate N, Sesti G, Frittitta L,**
964 **Marchetti P, Doria A, Trischitta V.** Joint Effect of Insulin Signaling Genes on Insulin
965 Secretion and Glucose Homeostasis. *J Clin Endocrinol Metab* 98: E1143–E1147, 2013.
- 966 52. **R Development Core Team.** A language and environment for statistical computing [Online]. R
967 Foundation for Statistical Computing. www.R-project.org.
- 968 53. **Rampoldi L, Dobson-Stone C, Rubio JP, Danek A, Chalmers RM, Wood NW, Verellen C,**
969 **Ferrer X, Malandrini A, Fabrizi GM, Brown R, Vance J, Pericak-Vance M, Rudolf G,**
970 **Carrè S, Alonso E, Manfredi M, Németh AH, Monaco AP.** A conserved sorting-associated
971 protein is mutant in chorea-acanthocytosis. *Nat Genet* 28: 119–120, 2001.
- 972 54. **Ravassard P, Hazhouz Y, Pechberty S, Bricout-Neveu E, Armanet M, Czernichow P,**
973 **Scharfmann R.** A genetically engineered human pancreatic β cell line exhibiting glucose-
974 inducible insulin secretion. *J Clin Invest* 121: 3589–3597, 2011.
- 975 55. **Ravier MA, Rutter GA.** Isolation and culture of mouse pancreatic islets for ex vivo imaging
976 studies with trappable or recombinant fluorescent probes. *Methods Mol Biol Clifton NJ* 633:
977 171–184, 2010.
- 978 56. **Rodriguez-Diaz R, Caicedo A.** Neural control of the endocrine pancreas. *Best Pract Res Clin*
979 *Endocrinol Metab* 28: 745–756, 2014.
- 980 57. **Rutter GA.** Dorothy Hodgkin Lecture 2014 Understanding genes identified by genome-wide
981 association studies for Type 2 diabetes. *Diabet Med* 31: 1480–1487, 2014.
- 982 58. **Rutter GA, Chimienti F.** SLC30A8 mutations in type 2 diabetes. *Diabetologia* 58: 31–36,
983 2014.
- 984 59. **Samaranayake HS, Cowan AE, Klobutcher LA.** Vacuolar Protein Sorting Protein 13A,
985 TtVPS13A, Localizes to the Tetrahymena thermophila Phagosome Membrane and Is Required
986 for Efficient Phagocytosis. *Eukaryot Cell* 10: 1207–1218, 2011.
- 987 60. **Saxena R, Hivert M-F, Langenberg C, Tanaka T, Pankow JS, Vollenweider P, Lyssenko**
988 **V, Bouatia-Naji N, Dupuis J, Jackson AU, Kao WHL, Li M, Glazer NL, Manning AK,**
989 **Luan J 'an, Stringham HM, Prokopenko I, Johnson T, Grarup N, Boesgaard TW, Lecoeur**
990 **C, Shrader P, O'Connell J, Ingelsson E, Couper DJ, Rice K, Song K, Andreasen CH, Dina**
991 **C, Köttgen A, Le Bacquer O, Pattou F, Taneera J, Steinthorsdottir V, Rybin D, Ardlie K,**
992 **Sampson M, Qi L, van Hoek M, Weedon MN, Aulchenko YS, Voight BF, Grallert H,**
993 **Balkau B, Bergman RN, Bielinski SJ, Bonnefond A, Bonnycastle LL, Borch-Johnsen K,**
994 **Böttcher Y, Brunner E, Buchanan TA, Bumpstead SJ, Cavalcanti-Proença C, Charpentier**
995 **G, Chen Y-DI, Chines PS, Collins FS, Cornelis M, Crawford GJ, Delplanque J, Doney A,**
996 **Egan JM, Erdos MR, Firmann M, Forouhi NG, Fox CS, Goodarzi MO, Graessler J,**
997 **Hingorani A, Isomaa B, Jørgensen T, Kivimaki M, Kovacs P, Krohn K, Kumari M,**
998 **Lauritzen T, Lévy-Marchal C, Mayor V, McAteer JB, Meyre D, Mitchell BD, Mohlke KL,**
999 **Morken MA, Narisu N, Palmer CNA, Pakyz R, Pascoe L, Payne F, Pearson D, Rathmann**
1000 **W, Sandbaek A, Sayer AA, Scott LJ, Sharp SJ, Sijbrands E, Singleton A, Siscovick DS,**
1001 **Smith NL, Sparso T, Swift AJ, Syddall H, Thorleifsson G, Tönjes A, Tuomi T, Tuomilehto**
1002 **J, Valle TT, Waeber G, Walley A, Waterworth DM, Zeggini E, Zhao JH, Consortium G,**
1003 **Investigators the M.** Genetic variation in GIPR influences the glucose and insulin responses to
1004 an oral glucose challenge. *Nat Genet* 42: 142–148, 2010.

- 1005 61. **Schaub MA, Boyle AP, Kundaje A, Batzoglou S, Snyder M.** Linking disease associations
1006 with regulatory information in the human genome. *Genome Res* 22: 1748–1759, 2012.
- 1007 62. **Seifert W, Kühnisch J, Maritzen T, Horn D, Haucke V, Hennies HC.** Cohen Syndrome-
1008 associated Protein, COH1, Is a Novel, Giant Golgi Matrix Protein Required for Golgi Integrity.
1009 *J Biol Chem* 286: 37665–37675, 2011.
- 1010 63. **Seifert W, Kühnisch J, Maritzen T, Lommatzsch S, Hennies HC, Bachmann S, Horn D,**
1011 **Haucke V.** Cohen Syndrome-associated Protein COH1 Physically and Functionally Interacts
1012 with the Small GTPase RAB6 at the Golgi Complex and Directs Neurite Outgrowth. *J Biol*
1013 *Chem* 290: 3349–3358, 2015.
- 1014 64. **Shiokawa N, Nakamura M, Sameshima M, Deguchi A, Hayashi T, Sasaki N, Sano A.**
1015 Chorein, the protein responsible for chorea-acanthocytosis, interacts with β -adducin and β -actin.
1016 *Biochem Biophys Res Commun* 441: 96–101, 2013.
- 1017 65. **Sladek R, Rocheleau G, Rung J, Dina C, Shen L, Serre D, Boutin P, Vincent D, Belisle A,**
1018 **Hadjadj S, Balkau B, Heude B, Charpentier G, Hudson TJ, Montpetit A, Pshezhetsky AV,**
1019 **Prentki M, Posner BI, Balding DJ, Meyre D, Polychronakos C, Froguel P.** A genome-wide
1020 association study identifies novel risk loci for type 2 diabetes. *Nature* 445: 881–885, 2007.
- 1021 66. **Stitzel ML, Huyghe JR, Morken MA, Parker SCJ, Fuchsberger C, Welch R, Jackson AU,**
1022 **Erdos MR, Kuusisto J, Laakso M, Boehnke M, Collins FS.** Fine-Mapping and Functional
1023 Genomic Analysis Link an Intergenic Islet Stretch Enhancer in the C2CD4A/B Locus to Islet
1024 Dysfunction. In: *Honing in on GWAS loci*. ADA 74th Scientific Sessions. San Francisco,
1025 California: 2014, p. A73.
- 1026 67. **Strawbridge RJ, Dupuis J, Prokopenko I, Barker A, Ahlqvist E, Rybin D, Petrie JR,**
1027 **Travers ME, Bouatia-Naji N, Dimas AS, Nica A, Wheeler E, Chen H, Voight BF, Taneera**
1028 **J, Kanoni S, Peden JF, Turrini F, Gustafsson S, Zabena C, Almgren P, Barker DJP,**
1029 **Barnes D, Dennison EM, Eriksson JG, Eriksson P, Eury E, Folkersen L, Fox CS, Frayling**
1030 **TM, Goel A, Gu HF, Horikoshi M, Isomaa B, Jackson AU, Jameson KA, Kajantie E,**
1031 **Kerr-Conte J, Kuulasmaa T, Kuusisto J, Loos RJJ, Luan J 'an, Makrilakis K, Manning**
1032 **AK, Martínez-Larrad MT, Narisu N, Mannila MN, Öhrvik J, Osmond C, Pascoe L, Payne**
1033 **F, Sayer AA, Sennblad B, Silveira A, Stančáková A, Stirrups K, Swift AJ, Syvänen A-C,**
1034 **Tuomi T, Hooft FM van 't, Walker M, Weedon MN, Xie W, Zethelius B, Consortium the**
1035 **D, Consortium the G, Consortium the M, Consortium the Cardi, Consortium the C,**
1036 **Ongen H, Mälarstig A, Hopewell JC, Saleheen D, Chambers J, Parish S, Danesh J, Kooner**
1037 **J, Östenson C-G, Lind L, Cooper CC, Serrano-Ríos M, Ferrannini E, Forsen TJ, Clarke**
1038 **R, Franzosi MG, Seedorf U, Watkins H, Froguel P, Johnson P, Deloukas P, Collins FS,**
1039 **Laakso M, Dermitzakis ET, Boehnke M, McCarthy MI, Wareham NJ, Groop L, Pattou F,**
1040 **Gloyn AL, Dedoussis GV, Lyssenko V, Meigs JB, Barroso I, Watanabe RM, Ingelsson E,**
1041 **Langenberg C, Hamsten A, Florez JC.** Genome-Wide Association Identifies Nine Common
1042 Variants Associated With Fasting Proinsulin Levels and Provides New Insights Into the
1043 Pathophysiology of Type 2 Diabetes. *Diabetes* 60: 2624–2634, 2011.
- 1044 68. **Thore S, Wuttke A, Tengholm A.** Rapid Turnover of Phosphatidylinositol-4,5-Bisphosphate in
1045 Insulin-Secreting Cells Mediated by Ca^{2+} and the ATP-to-ADP Ratio. *Diabetes* 56: 818–826,
1046 2007.
- 1047 69. **Thorens B, Tarussio D, Maestro MA, Rovira M, Heikkilä E, Ferrer J.** Ins1 Cre knock-in
1048 mice for beta cell-specific gene recombination. *Diabetologia* 58: 558–565, 2014.
- 1049 70. **Tomiyasu A, Nakamura M, Ichiba M, Ueno S, Saiki S, Morimoto M, Kobal J, Kageyama**
1050 **Y, Inui T, Wakabayashi K, Yamada T, Kanemori Y, Jung HH, Tanaka H, Orimo S, Afawi**

- 1051 **Z, Blatt I, Aasly J, Ujike H, Babovic-Vuksanovic D, Josephs KA, Tohge R, Rodrigues GR,**
 1052 **Dupré N, Yamada H, Yokochi F, Kotschet K, Takei T, Rudzińska M, Szczudlik A, Penco**
 1053 **S, Fujiwara M, Tojo K, Sano A.** Novel pathogenic mutations and copy number variations in
 1054 the VPS13A Gene in patients with chorea-acanthocytosis. *Am J Med Genet B Neuropsychiatr*
 1055 *Genet* 156: 620–631, 2011.
- 1056 71. **Ueno S, Maruki Y, Nakamura M, Tomemori Y, Kamae K, Tanabe H, Yamashita Y,**
 1057 **Matsuda S, Kaneko S, Sano A.** The gene encoding a newly discovered protein, chorein, is
 1058 mutated in chorea-acanthocytosis. *Nat Genet* 28: 121–122, 2001.
- 1059 72. **Velayos Baeza A, Dobson-Stone C, Rampoldi L, Bader B, Walker RH, Danek A, Monaco**
 1060 **AP.** Chorea-Acanthocytosis [Online]. In: *GeneReviews*(®), edited by Pagon RA, Adam MP,
 1061 Ardinger HH, Wallace SE, Amemiya A, Bean LJ, Bird TD, Fong C-T, Mefford HC, Smith RJ,
 1062 Stephens K. University of Washington, Seattle <http://www.ncbi.nlm.nih.gov/books/NBK1387/>
 1063 [12 Jan. 2016].
- 1064 73. **Velayos-Baeza A, Vettori A, Copley RR, Dobson-Stone C, Monaco AP.** Analysis of the
 1065 human VPS13 gene family. *Genomics* 84: 536–549, 2004.
- 1066 74. **Wallace TM, Levy JC, Matthews DR.** Use and Abuse of HOMA Modeling. *Diabetes Care* 27:
 1067 1487–1495, 2004.
- 1068 75. **Wang YJ, Wang J, Sun HQ, Martinez M, Sun YX, Macia E, Kirchhausen T, Albanesi JP,**
 1069 **Roth MG, Yin HL.** Phosphatidylinositol 4 phosphate regulates targeting of clathrin adaptor
 1070 AP-1 complexes to the Golgi. *Cell* 114: 299–310, 2003.
- 1071 76. **Weedon MN, Cebola I, Patch A-M, Flanagan SE, De Franco E, Caswell R, Rodríguez-**
 1072 **Seguí SA, Shaw-Smith C, Cho CH-H, Allen HL, Houghton JAL, Roth CL, Chen R,**
 1073 **Hussain K, Marsh P, Vallier L, Murray A, International Pancreatic Agenesis Consortium,**
 1074 **Ellard S, Ferrer J, Hattersley AT.** Recessive mutations in a distal PTF1A enhancer cause
 1075 isolated pancreatic agenesis. *Nat Genet* 46: 61–64, 2014.
- 1076 77. **Wicksteed B, Brissova M, Yan W, Opland DM, Plank JL, Reinert RB, Dickson LM,**
 1077 **Tamarina NA, Philipson LH, Shostak A, Bernal-Mizrachi E, Elghazi L, Roe MW, Labosky**
 1078 **PA, Myers MG, Gannon M, Powers AC, Dempsey PJ.** Conditional Gene Targeting in Mouse
 1079 Pancreatic β -Cells Analysis of Ectopic Cre Transgene Expression in the Brain. *Diabetes* 59:
 1080 3090–3098, 2010.
- 1081 78. **Windholz J, Kovacs P, Tönjes A, Dittrich K, Blüher S, Kiess W, Stumvoll M, Körner A.**
 1082 Effects of Genetic Variants in ADCY5, GIPR, GCKR and VPS13C on Early Impairment of
 1083 Glucose and Insulin Metabolism in Children. *PLoS ONE* 6: e22101, 2011.
- 1084 79. **Wuttke A.** Lipid Signalling Dynamics at the β -cell Plasma Membrane. *Basic Clin Pharmacol*
 1085 *Toxicol* 116: 281–290, 2015.
- 1086 80. **Wuttke A, Sâgetorp J, Tengholm A.** Distinct plasma-membrane PtdIns(4)P and PtdIns(4,5)P2
 1087 dynamics in secretagogue-stimulated β -cells. *J Cell Sci* 123: 1492–1502, 2010.
- 1088 81. **Xavier G da S, Loder MK, McDonald A, Tarasov AI, Carzaniga R, Kronenberger K, Barg**
 1089 **S, Rutter GA.** TCF7L2 Regulates Late Events in Insulin Secretion From Pancreatic Islet β -
 1090 Cells. *Diabetes* 58: 894–905, 2009.
- 1091 82. **Xavier G da S, Mondragon A, Sun G, Chen L, McGinty JA, French PM, Rutter GA.**
 1092 Abnormal glucose tolerance and insulin secretion in pancreas-specific Tcf7l2-null mice.
 1093 *Diabetologia* 55: 2667–2676, 2012.

1094 83. **Yamauchi T, Hara K, Maeda S, Yasuda K, Takahashi A, Horikoshi M, Nakamura M,**
1095 **Fujita H, Grarup N, Cauchi S, Ng DPK, Ma RCW, Tsunoda T, Kubo M, Watada H,**
1096 **Maegawa H, Okada-Iwabu M, Iwabu M, Shojima N, Shin HD, Andersen G, Witte DR,**
1097 **Jørgensen T, Lauritzen T, Sandbæk A, Hansen T, Ohshige T, Omori S, Saito I, Kaku K,**
1098 **Hirose H, So W-Y, Beury D, Chan JCN, Park KS, Tai ES, Ito C, Tanaka Y, Kashiwagi A,**
1099 **Kawamori R, Kasuga M, Froguel P, Pedersen O, Kamatani N, Nakamura Y, Kadowaki T.**
1100 A genome-wide association study in the Japanese population identifies susceptibility loci for
1101 type 2 diabetes at UBE2E2 and C2CD4A-C2CD4B. *Nat Genet* 42: 864–868, 2010.

1102 84. **Yang R-Y, Xue H, Yu L, Velayos-Baeza A, Monaco AP, Liu F-T.** Identification of VPS13C
1103 as a Galectin-12-Binding Protein That Regulates Galectin-12 Protein Stability and
1104 Adipogenesis. *PLOS ONE* 11: e0153534, 2016.

1105 85. **Zhang B, Chang A, Kjeldsen TB, Arvan P.** Intracellular Retention of Newly Synthesized
1106 Insulin in Yeast Is Caused by Endoproteolytic Processing in the Golgi Complex. *J Cell Biol*
1107 153: 1187–1198, 2001.

1108 86. **Zhang C, Qi L, Hunter DJ, Meigs JB, Manson JE, Dam RM van, Hu FB.** Variant of
1109 Transcription Factor 7-Like 2 (TCF7L2) Gene and the Risk of Type 2 Diabetes in Large
1110 Cohorts of U.S. Women and Men. *Diabetes* 55: 2645–2648, 2006.

1111 87. Diabetes risk factors - Diabetes UK [Online]. [date unknown].
1112 [https://www.diabetes.org.uk/Guide-to-diabetes/What-is-diabetes/Know-your-risk-of-Type-2-](https://www.diabetes.org.uk/Guide-to-diabetes/What-is-diabetes/Know-your-risk-of-Type-2-diabetes/Diabetes-risk-factors/)
1113 [diabetes/Diabetes-risk-factors/](https://www.diabetes.org.uk/Guide-to-diabetes/What-is-diabetes/Know-your-risk-of-Type-2-diabetes/Diabetes-risk-factors/) [21 Jan. 2016].

1114

1115

1116

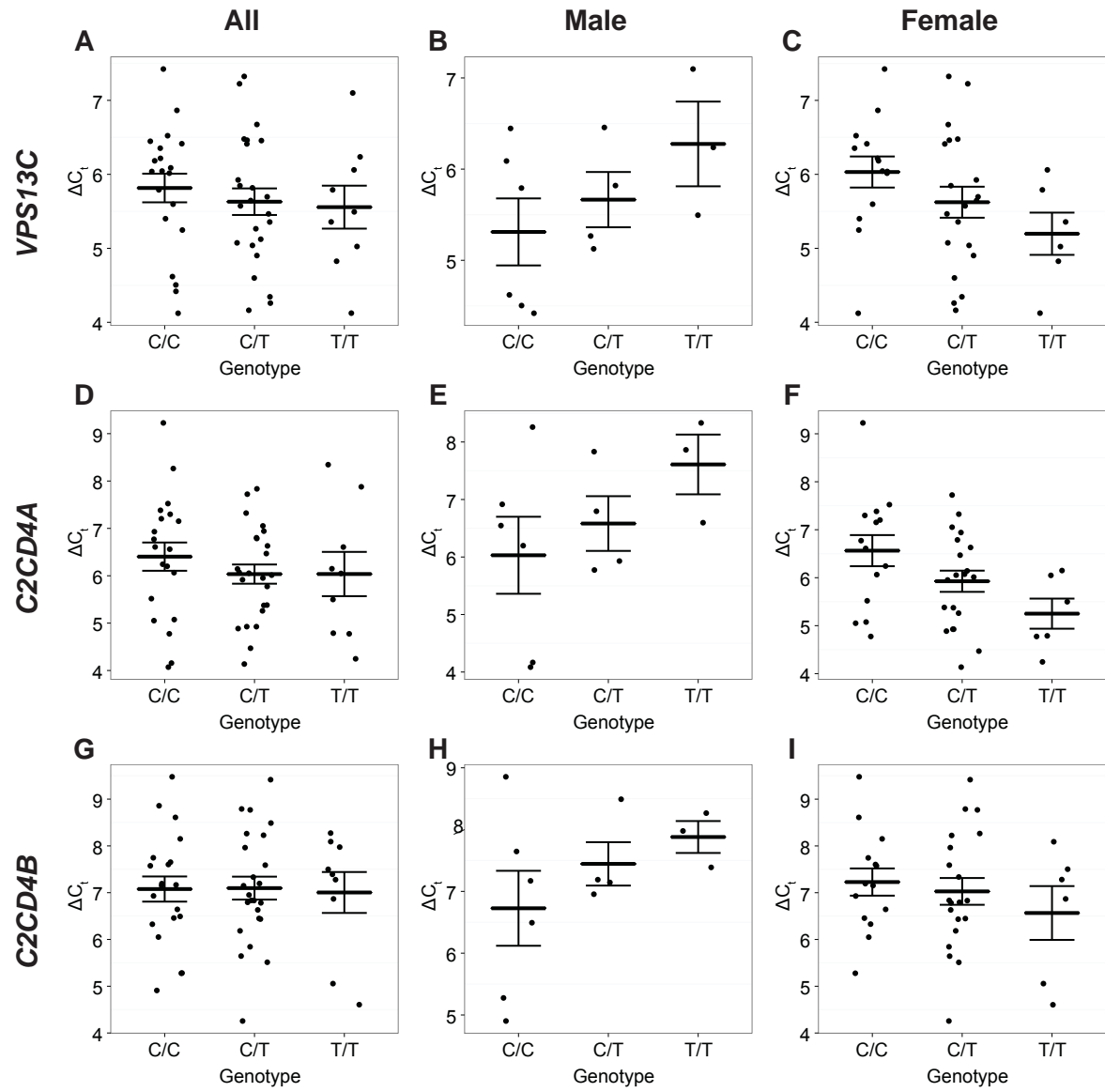


Figure 1

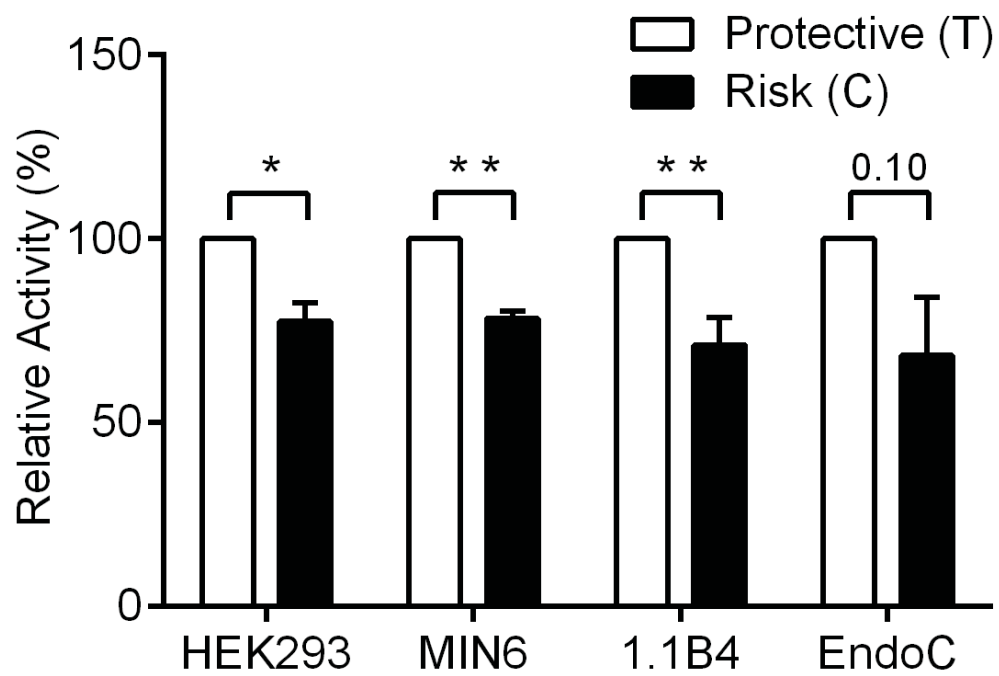


Figure 2

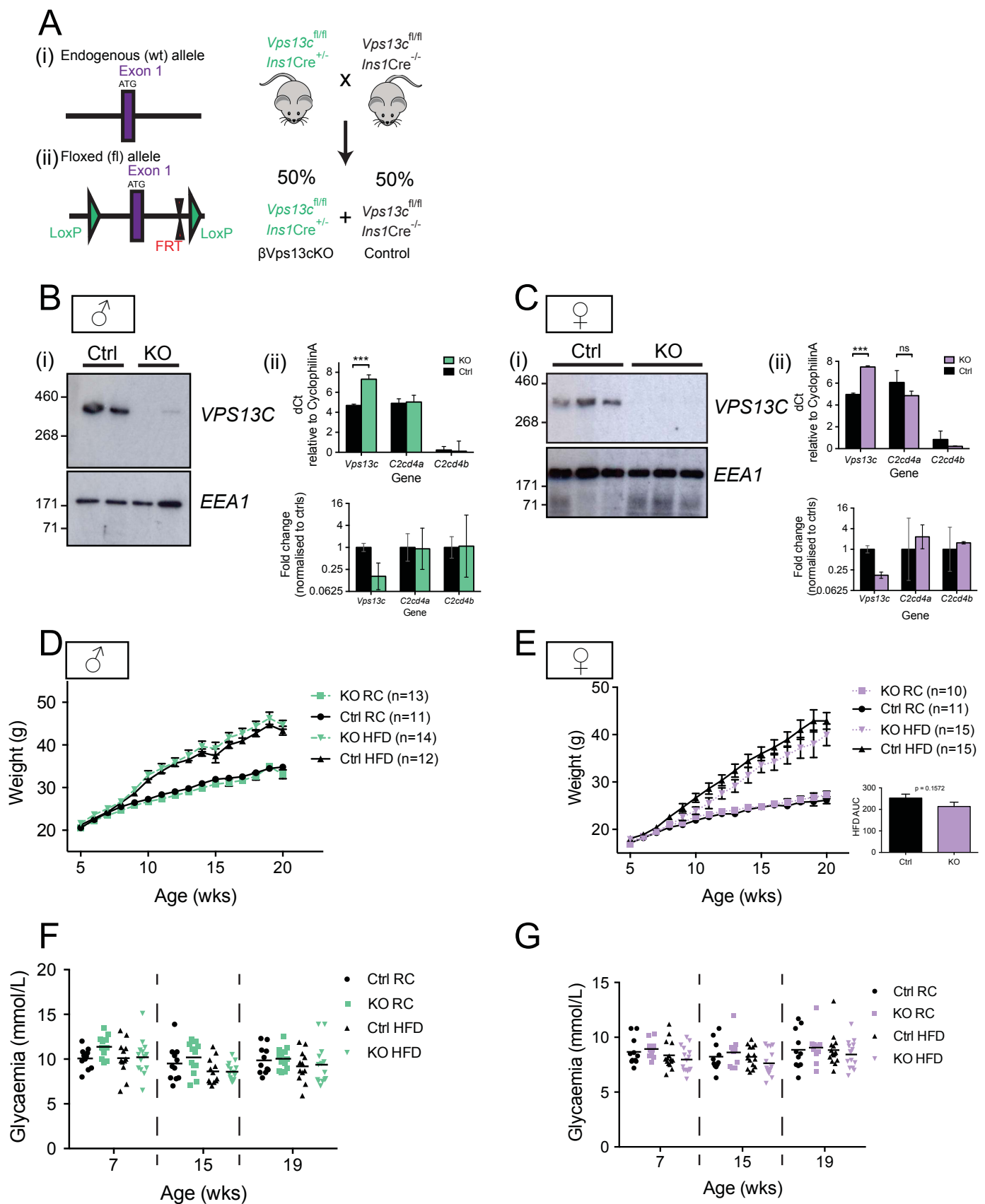


Figure 3

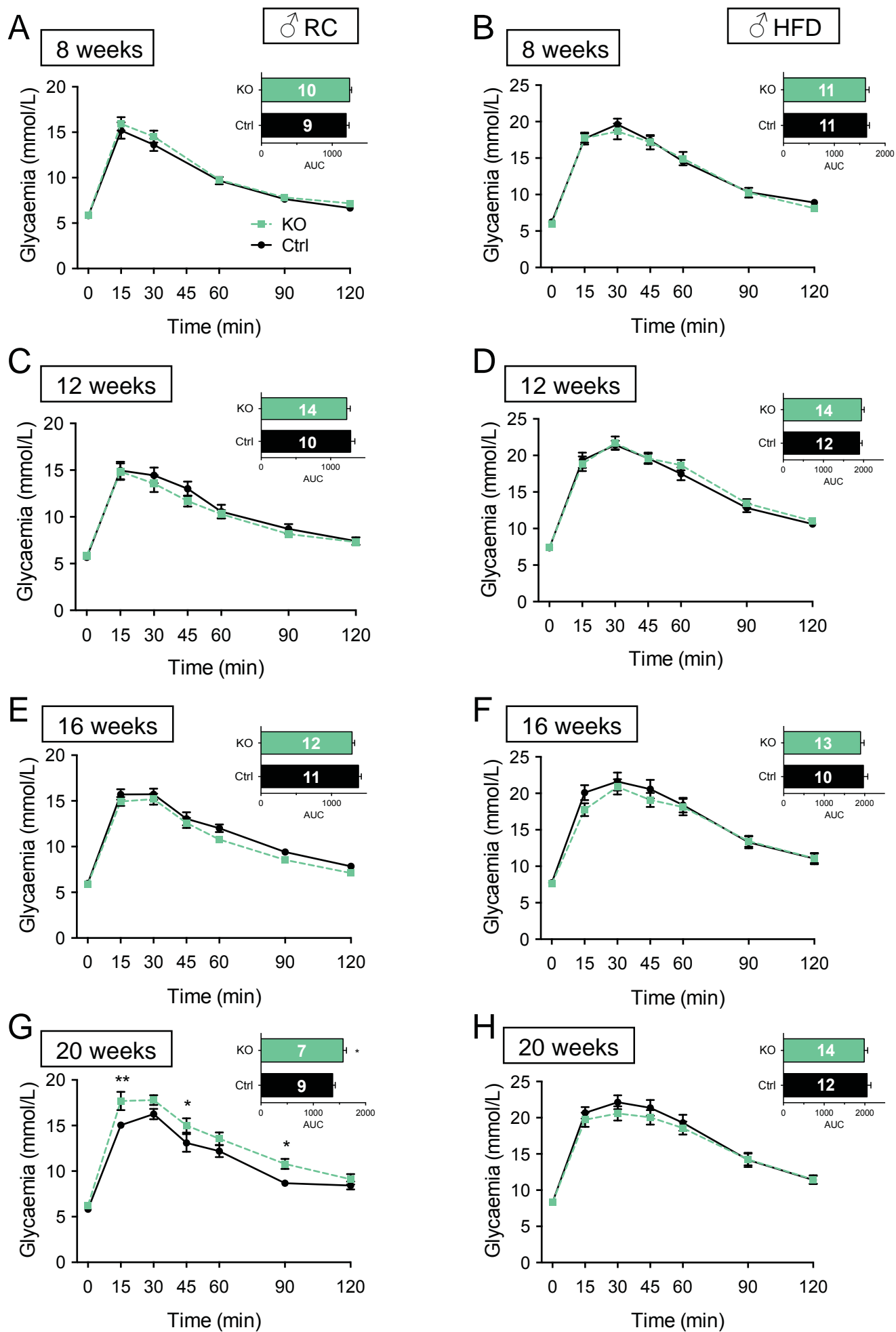


Figure 4

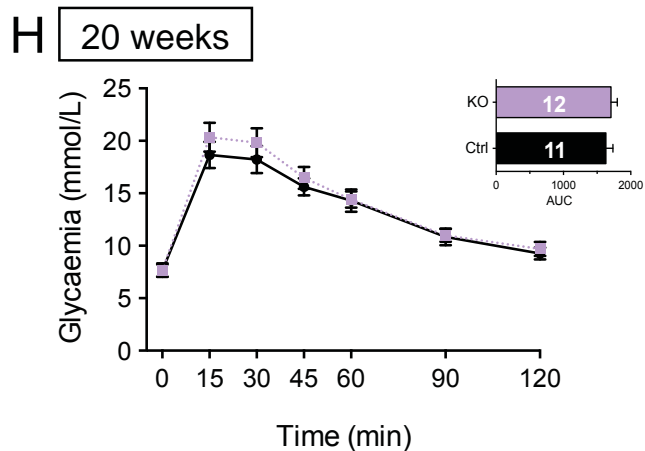
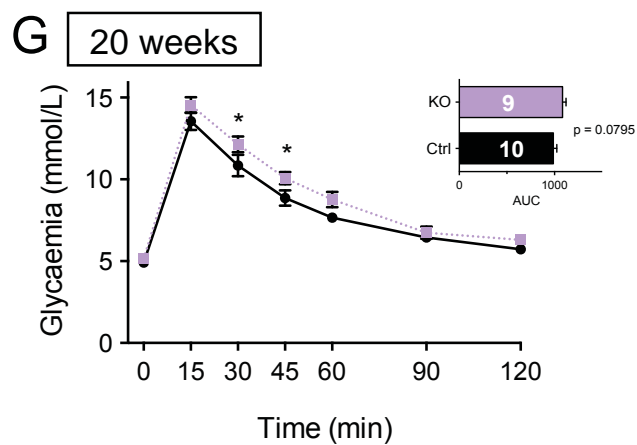
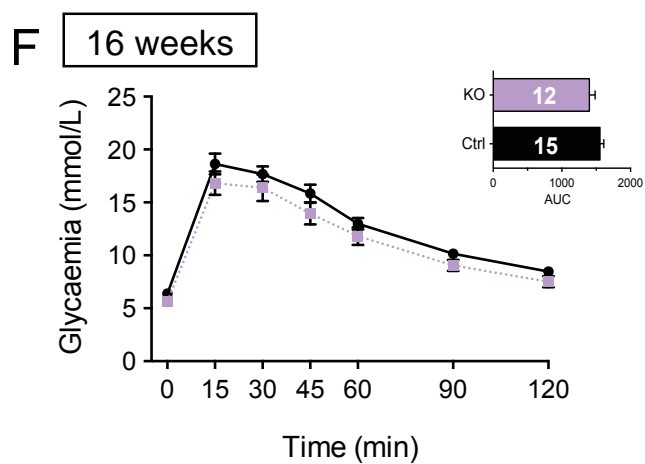
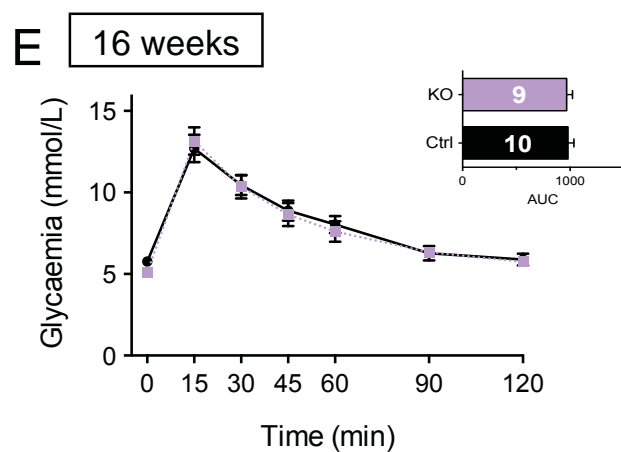
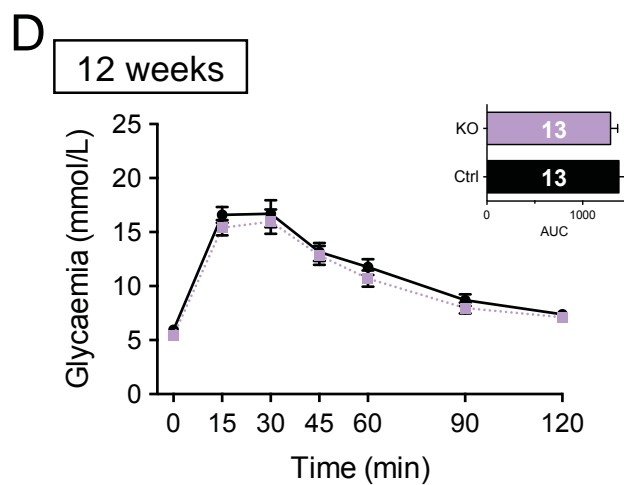
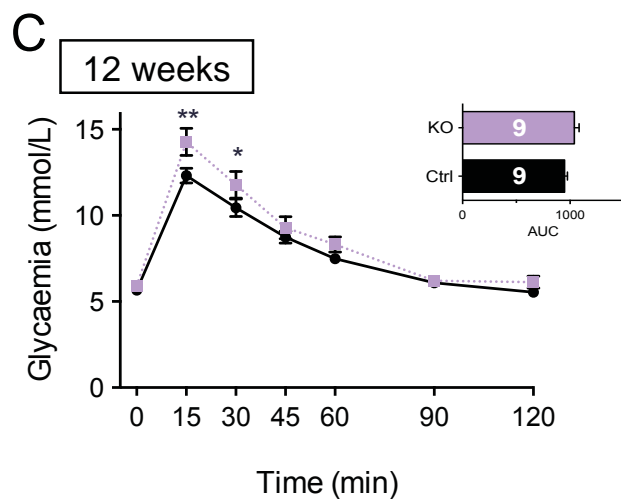
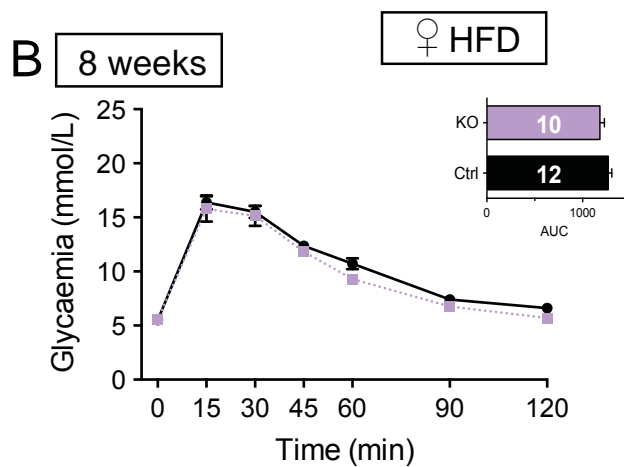
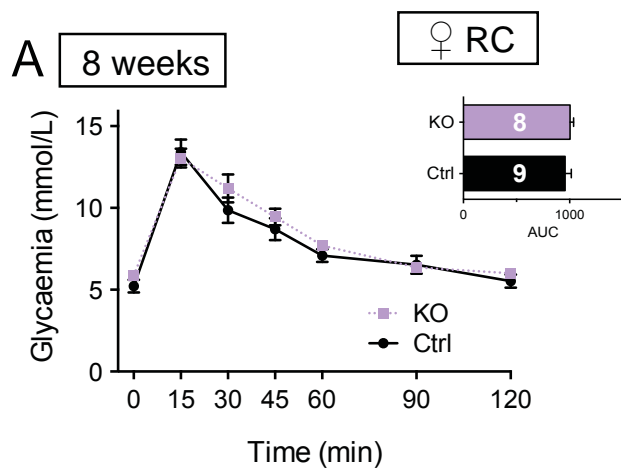


Figure 5

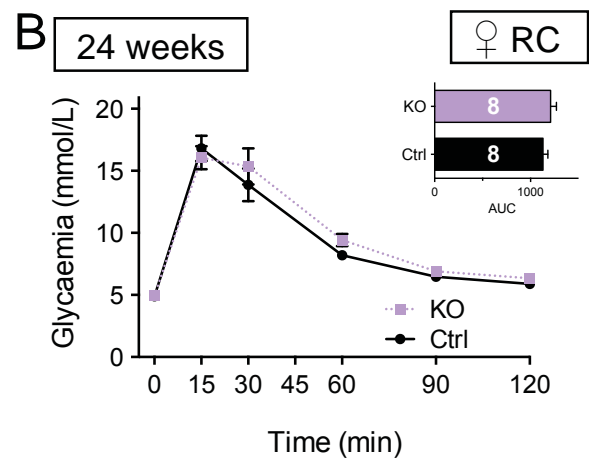
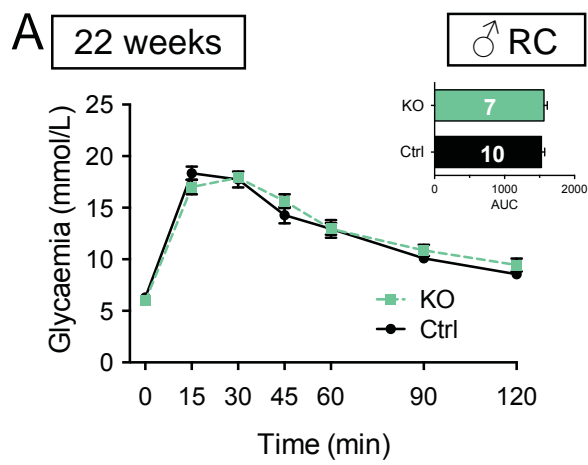


Figure 6

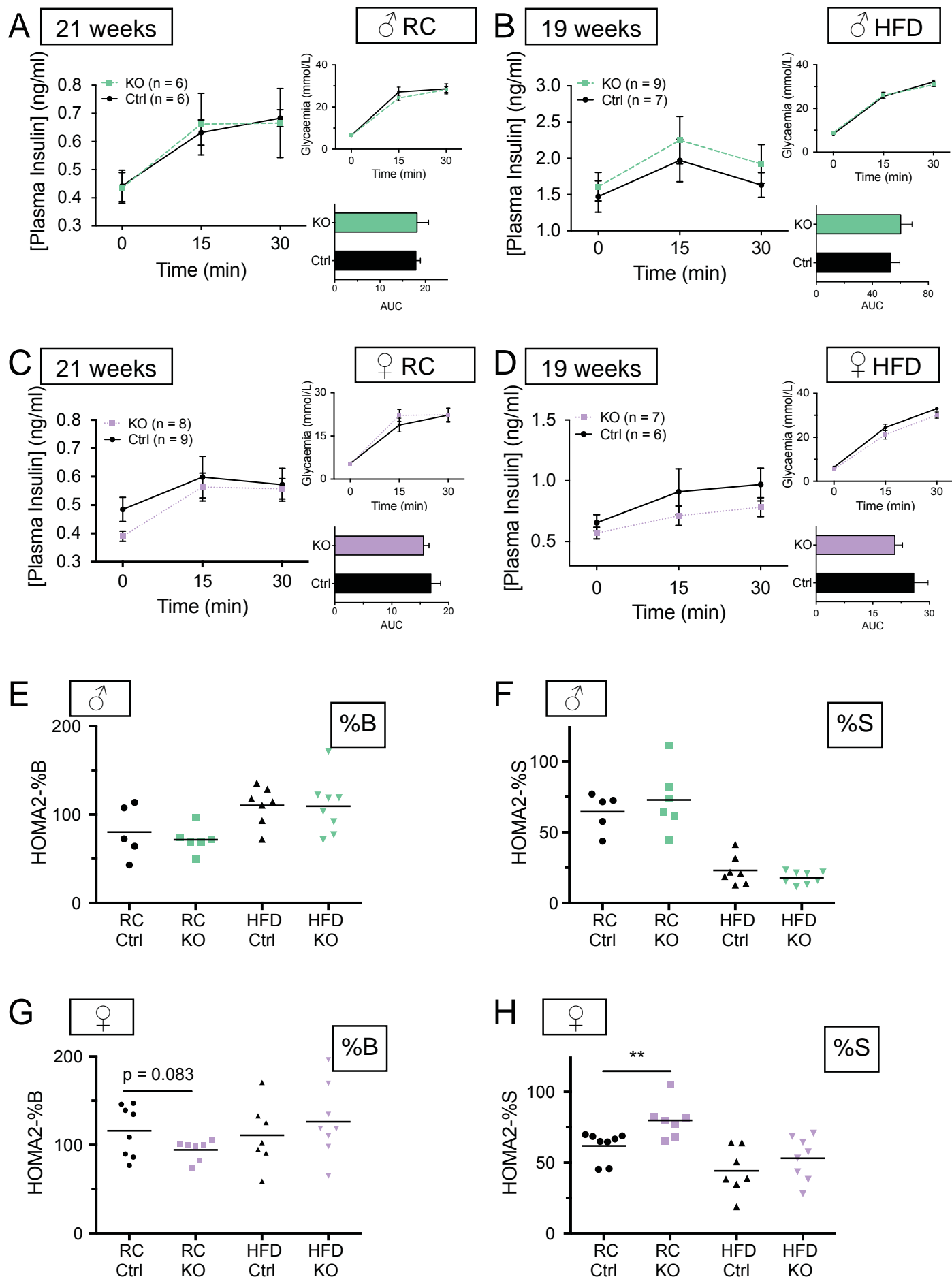


Figure 7

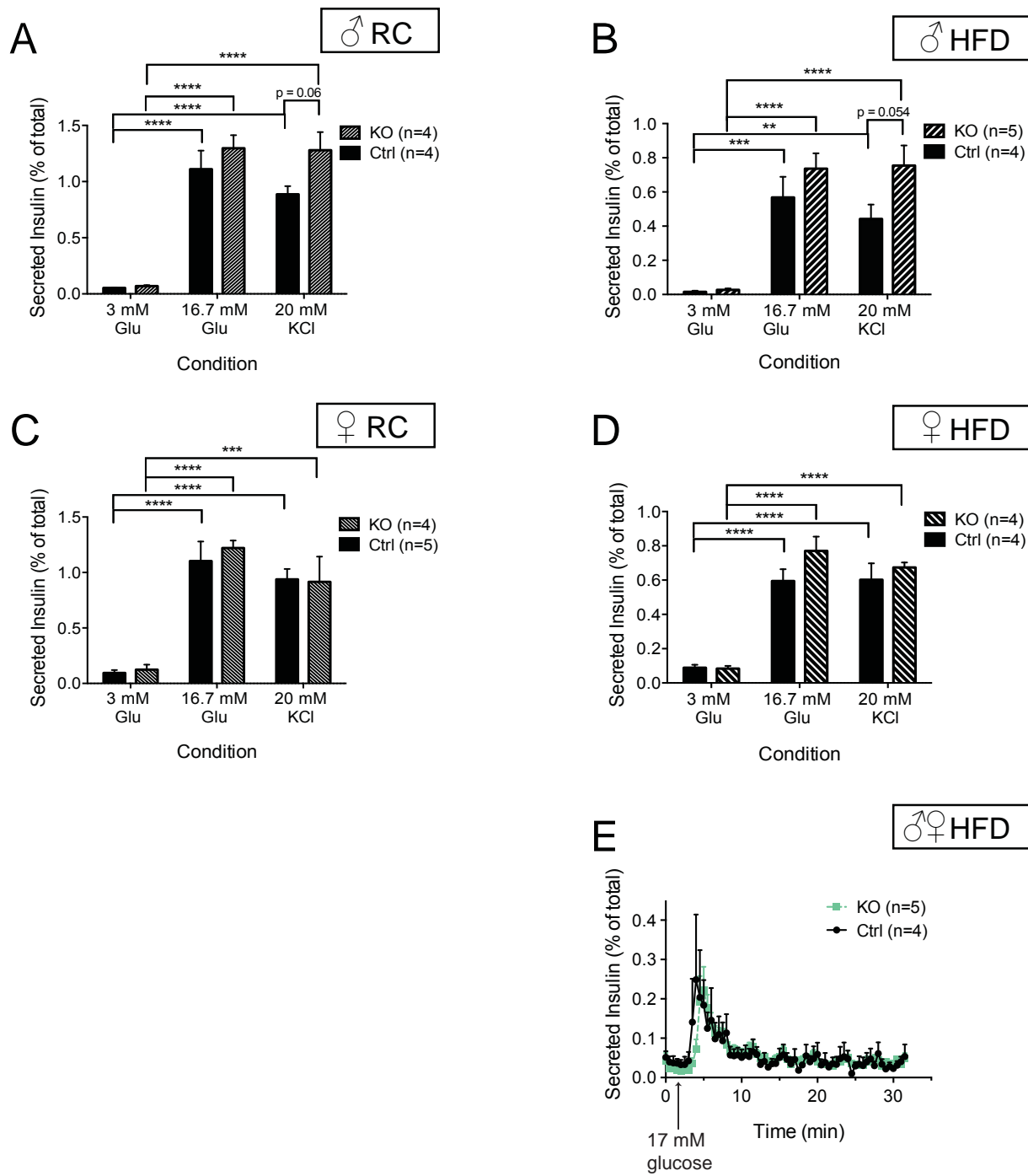
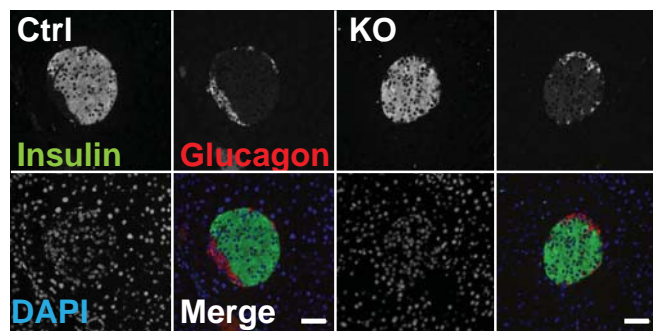
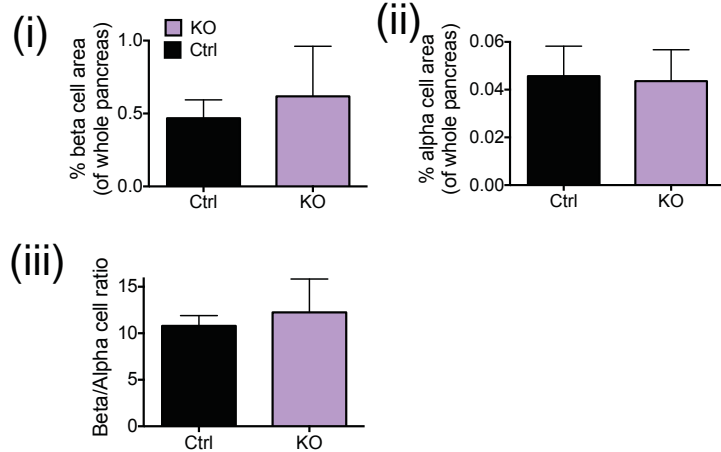


Figure 8

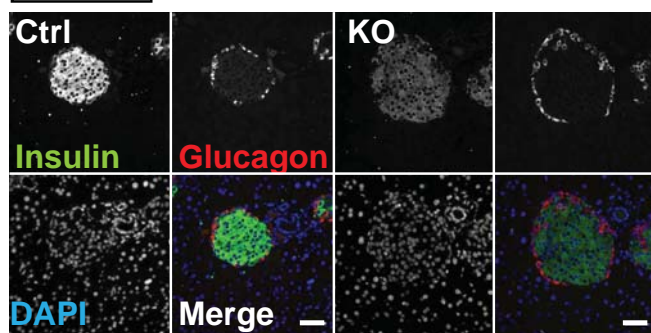
A ♀ RC



B



C ♂ RC



D

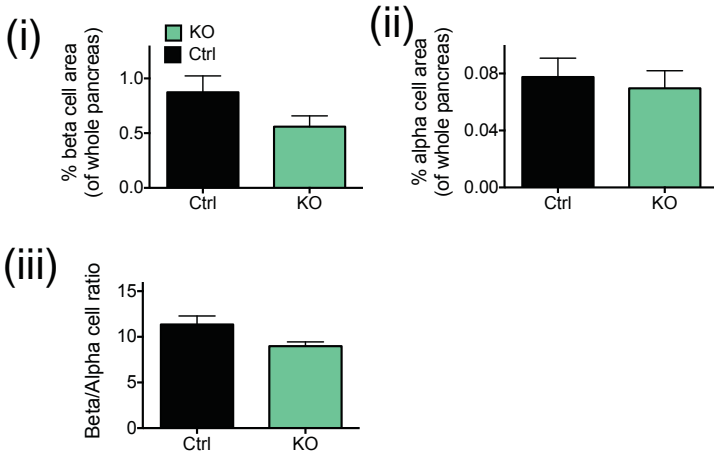


Figure 9

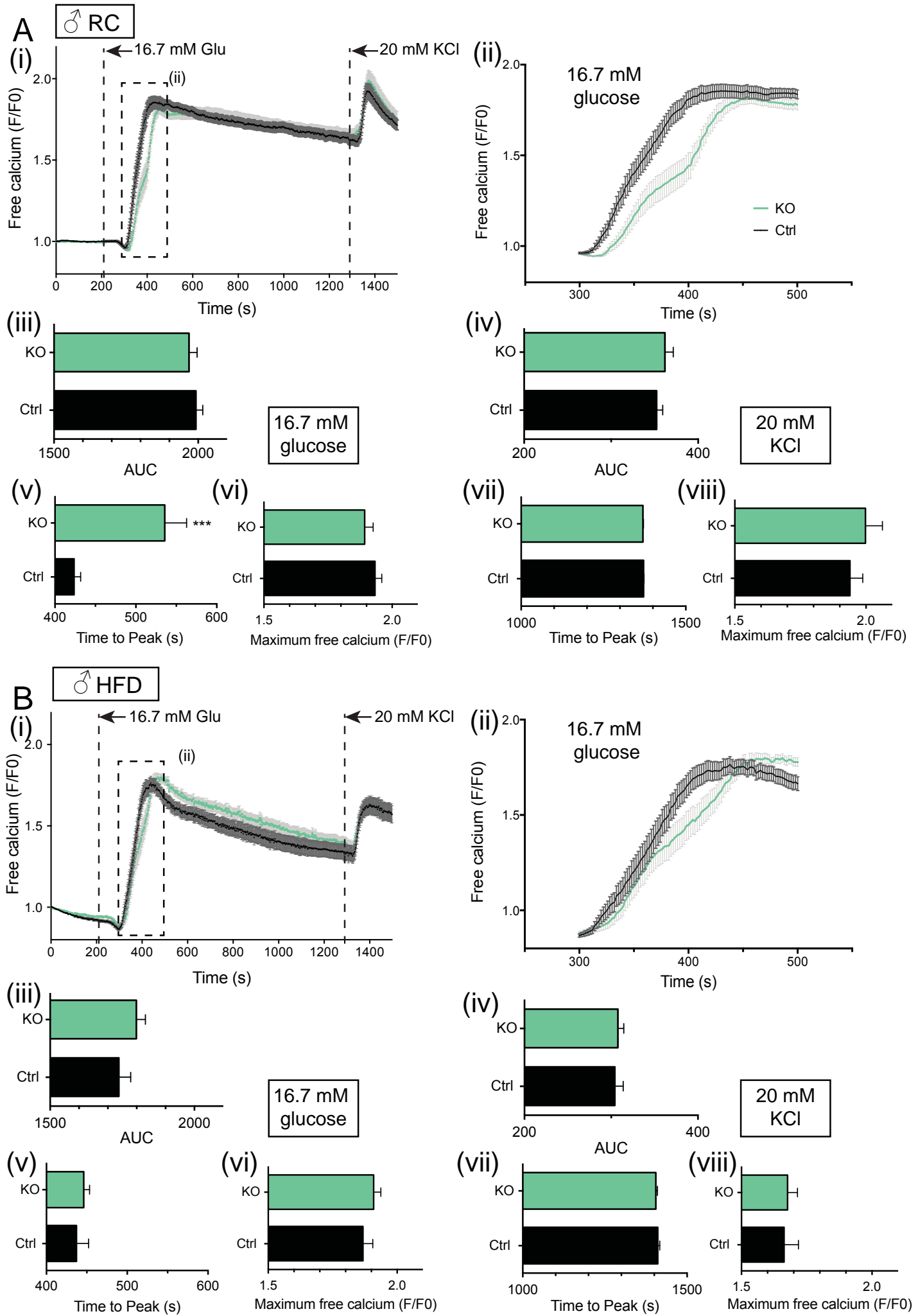


Figure 10

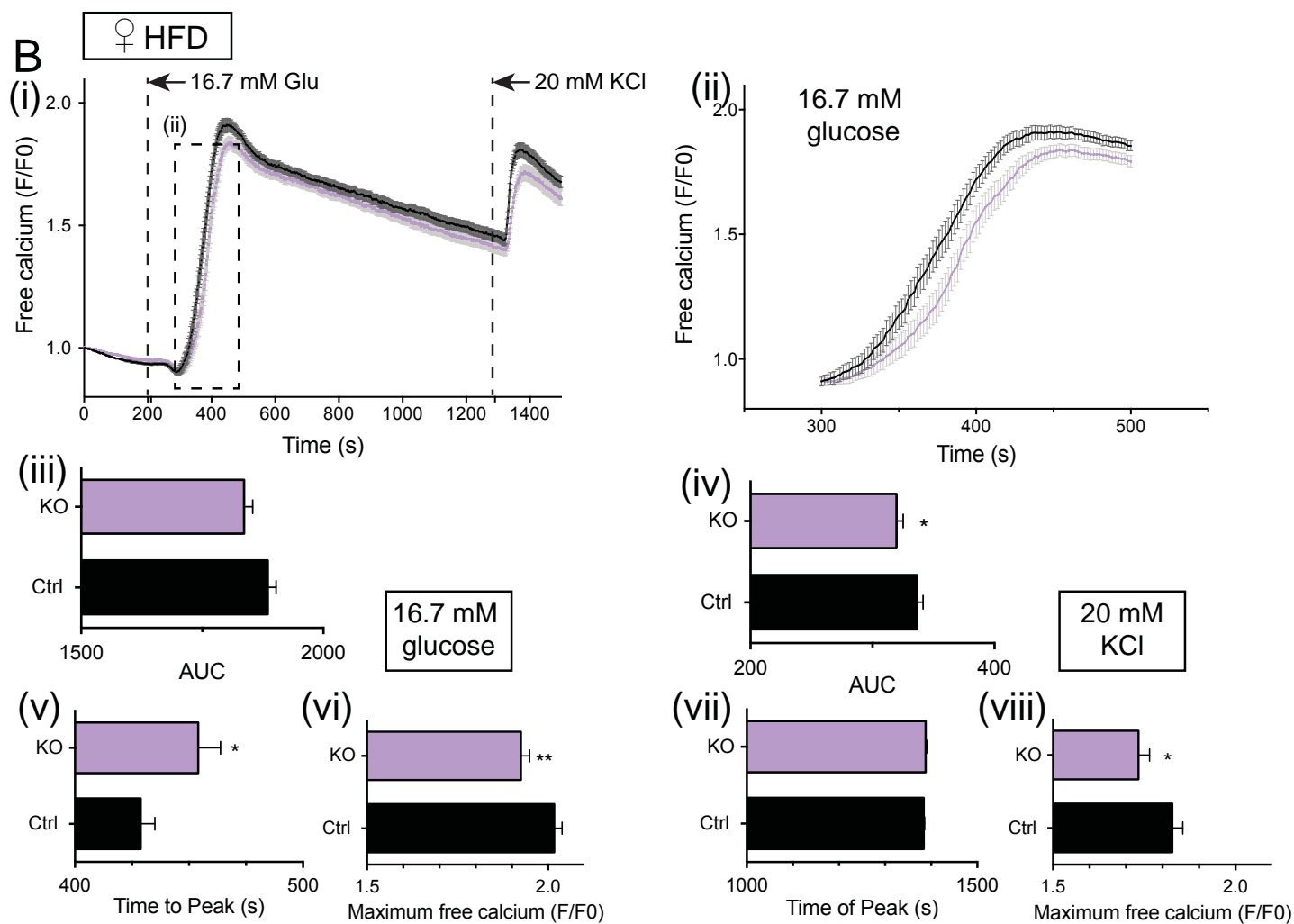
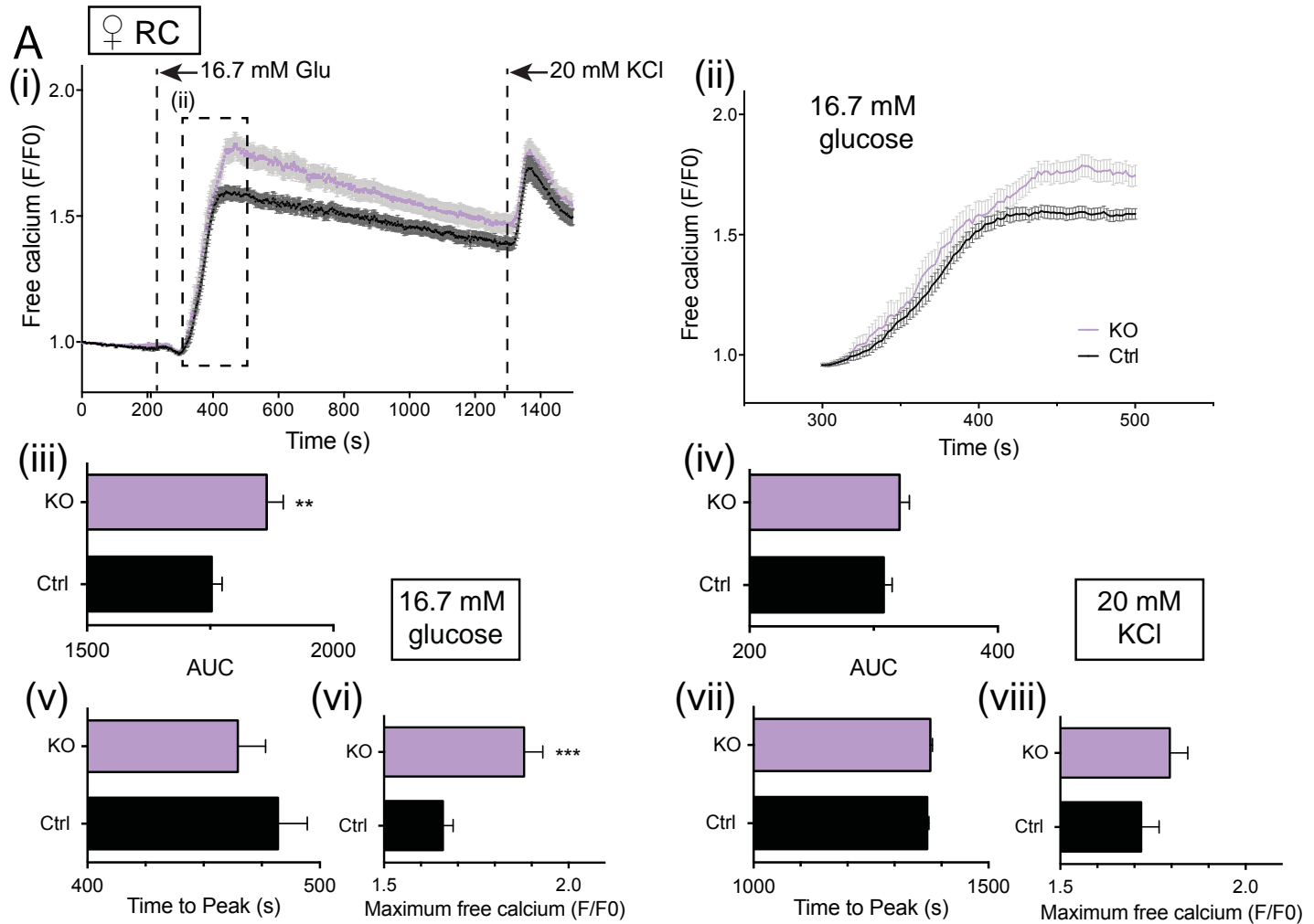


Figure 11

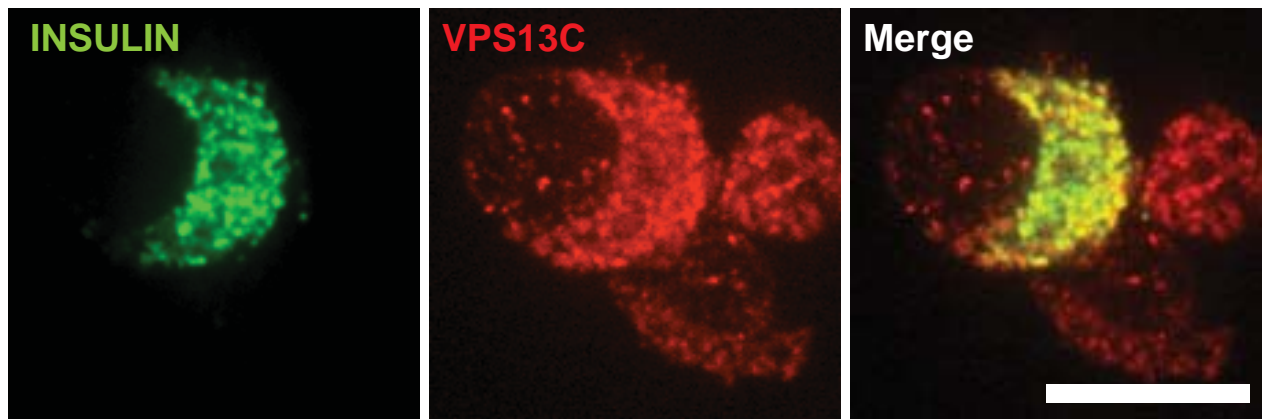
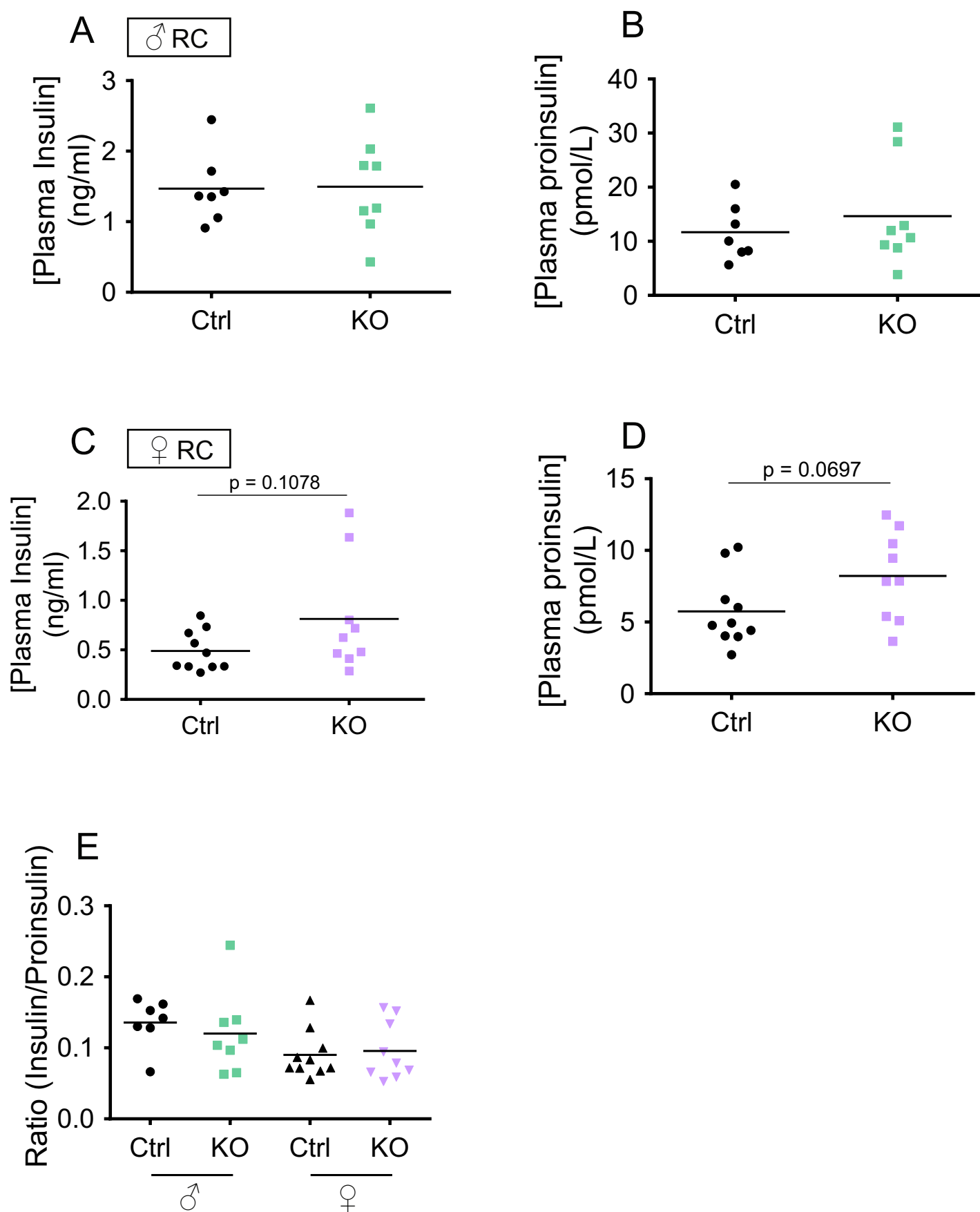


Figure 12

Supplementary Figure 1 legend: Random-fed insulin and proinsulin plasma concentrations in RC-fed mice. Plasma insulin and proinsulin were measured following collection from the tail vein (before culling) and aorta (immediately post-mortem) of RC-fed control (black) or $\beta Vps13c$ KO (green, males (A and B); purple, females (C and D)) mice aged over 21 weeks old. The ratio of [plasma insulin]/[plasma proinsulin] is shown in E. $n = 7$ ctrl and 8 KO (males); 10 ctrl and 9 KO (females).



Supplementary Methods

Image analysis

(1) β and α cell mass

In order to quantify alpha and beta cell mass a signal threshold was first applied on images stained for glucagon to determine surface occupied by glucagon-positive cells. The surface area is calculated as follows: the “thresholded” image is converted to mask, then “analyse particles” is performed. The surface of each particle is determined and all particle surfaces are then added together.

The same treatment is applied to the corresponding image stained for insulin. The ratio of surface is then calculated. Note that the ratio is a surface ratio: fluorescence intensity level is not taken into account in the calculation.

Macro script:

```
// step 0 : set up parameters - clear up roi manager
```

```
run("Set Measurements...", "area mean min integrated redirect=None decimal=0");
```

```
run("Options...", "iterations=3 count=1 black edm=Overwrite do=Nothing");
```

```
roiManager("reset");
```

```
run("Close All");
```

```
run("Clear Results");
```

```
//step 1 : indicate the folder containing the images to analyse
```

```
dir=getDirectory("Where are the images?");
```

```
file=getFileList(dir);
```

```
File.makeDirectory(dir+"results");
```

```
Resultats = File.open(dir+File.separator+"results"+File.separator+"Results.xls");
```

```
entete = "Image name\tSurface alpha cells\tSurface beta cells\tRatio alpha/beta \n";
```

```
print(Resultats, entete);
```

```
// step 1 bis : open the image to analyse
```

```
for(i = 0 ; i< file.length ; i++) {
```

```
if(lastIndexOf(file[i], ".ome")!= -1){
```

```
open(file[i]);
```

```
image = getTitle();
```

```
// step 2 determination surface alpha
```

```
Stack.setChannel(3);
```

```
alpha = surfaceDetermin(image, dir);
```

```
run("Clear Results");
```

```
run("Select None");
```

```
if( alpha != 0) {
```

```
roiManager("Save", dir+File.separator+ "results"+File.separator+ image+"Roiset-areaAlpha.zip");
```

```
}
```

```
roiManager("reset");
```

```
// step 3 determination surface beta
```

```
selectWindow(image);
```

```
Stack.setChannel(2);
```

```
beta = surfaceDetermin(image, dir);
```

```
run("Clear Results");
```

```
run("Select None");
```

```
roiManager("Save", dir+File.separator+ "results"+File.separator+ image+"Roiset-areaBeta.zip");  
roiManager("reset");
```

```
// step 4 : put data in the results file - close image and duplicats
```

```
ratio = alpha/beta;
```

```
if (ratio == 0) {  
    ligne = image + "\t" + "no alpha cells" + "\t" + beta + "\t" + ratio + "\n";  
} else {  
    ligne = image + "\t" + alpha + "\t" + beta + "\t" + ratio + "\n";  
}  
print(Resultats, ligne);  
run("Close All");  
}  
}
```

```
File.close(Resultats);
```

```
//-----
```

```
function surfaceDetermin(image, dir) {
```

```
    run("Duplicate...", "title= duplicat1");
```

```
    run("Threshold...");
```

```
    setAutoThreshold("Default dark");
```

```
    waitForUser("Adjust threshold");
```

```
    run("Convert to Mask");
```



```
run("Close-");

run("Analyze Particles...", "size=10-Infinity circularity=0.00-1.00 show=Nothing display clear
include add ");
```

```
surface = 0 ;
```

```
nbRoi = roiManager("Count");
```

```
for (i = 0; i < nbRoi; i++)
```

```
{
```

```
surface = surface + getResult("Area", i);
```

```
}
```

```
return surface;
```

```
}
```

Ca²⁺ Imaging with fluo2

The trappable intracellular probe fluo-2 (10uM) was loaded for 45 minutes. Acquisitions were then performed at a rate of 30 images per minutes on a spinning disc microscope as described under Methods. Acquired films were analysed using the macro (script following).

Briefly, a “max intensity” projection is performed with the 500 first images of the stack to have a clear image for threshold. The threshold is applied on the projected image to distinguish fluorescence signal from islets versus background.

The user is asked to draw an area around each islet in the field of view. For each islet, mean fluorescence intensity is determined for each time point on the original stack. Results are recorded in an Excel spreadsheet.

Each trace thus represents the average fluorescence intensity measured for one islet along time.

Macro script

```
// step 0 : set up parameters - clear up roi manager
```

```
run("Set Measurements...", "mean redirect=None decimal=2");
```

```
run("Options...", "iterations=1 count=1 black edm=Overwrite do=Nothing");
```

```
roiManager("reset");
```

```
//run("Close All");
```

```
run("Clear Results");
```

```
waitForUser("Open your image");
```

```
image = getTitle();
```

```
dir=getDirectory("Where do you want to save the results?");
```

```
selectWindow(image);
```

```
run("Z Project...", "stop=500 projection=[Max Intensity]");
```

```
setAutoThreshold("Default dark");
```

```
waitForUser("Check threshold");
```

```
setOption("BlackBackground", true);
```

```
run("Convert to Mask");
```

```
run("Close-");
```

```
saveAs("Tiff", dir+File.separator+ image + "_mask");
```

```
otsu = getTitle();
```

```
Dialog.create(" How many islets analysable?");
```

```
Dialog.addNumber("nb d'ilot", 1);
```

```
Dialog.show();
```

```
nbilot = Dialog.getNumber();
```

```
for (i=1; i<= nbilot; i++) {

selectWindow(otsu);

waitForUser(" draw ROI around the ilet " + i);


run("Analyze Particles...", "size=100-Infinity pixel clear include add");


selectWindow(image);

roiManager("Deselect");

roiManager("Multi Measure");

saveAs("Results", dir+File.separator + "Results-ilot"+ i + ".xls");

roiManager("Save", dir+ File.separator + "RoiSet-ilot"+i+".zip");


roiManager("Reset");

run("Clear Results");

}


run("Close All");
```